# 

Cite as: Chem. Phys. Rev. **2**, 031301 (2021); https://doi.org/10.1063/5.0049111 Submitted: 01 March 2021 . Accepted: 08 June 2021 . Published Online: 08 July 2021

Zhantao Chen, Nina Andrejevic, Nathan C. Drucker, Thanh Nguyen, D R. Patrick Xian, D Tess Smidt, D Yao Wang, Ralph Ernstorfer, D D. Alan Tennant, Maria Chan, and Mingda Li

#### **COLLECTIONS**

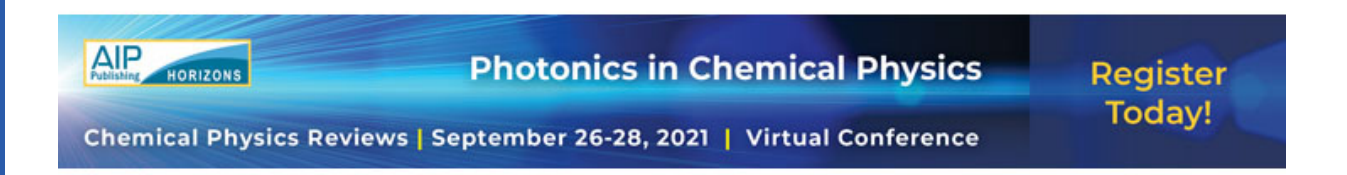
- F This paper was selected as Featured
- SCI This paper was selected as Scilight













# Machine learning on neutron and x-ray scattering and spectroscopies (5) (6)

Cite as: Chem. Phys. Rev. 2, 031301 (2021); doi: 10.1063/5.0049111

Submitted: 1 March 2021 · Accepted: 8 June 2021 ·

Published Online: 8 July 2021







Zhantao Chen,<sup>1,2</sup> Nina Andrejevic,<sup>1,3</sup> Nathan C. Drucker,<sup>1,4</sup> Thanh Nguyen,<sup>1,5</sup> R. Patrick Xian,<sup>6</sup> Tess Smidt,<sup>7</sup> Nao Wang,<sup>8</sup> Ralph Ernstorfer,<sup>6</sup> D. Alan Tennant,<sup>9</sup> Denant,<sup>10</sup> Maria Chan,<sup>10</sup> Denand Mingda Li<sup>1,5,a)</sup> Denand Mingda Li<sup>1,5</sup>

#### **AFFILIATIONS**

#### **ABSTRACT**

Neutron and x-ray scattering represent two classes of state-of-the-art materials characterization techniques that measure materials structural and dynamical properties with high precision. These techniques play critical roles in understanding a wide variety of materials systems from catalysts to polymers, nanomaterials to macromolecules, and energy materials to quantum materials. In recent years, neutron and x-ray scattering have received a significant boost due to the development and increased application of machine learning to materials problems. This article reviews the recent progress in applying machine learning techniques to augment various neutron and x-ray techniques, including neutron scattering, x-ray absorption, x-ray scattering, and photoemission. We highlight the integration of machine learning methods into the typical workflow of scattering experiments, focusing on problems that challenge traditional analysis approaches but are addressable through machine learning, including leveraging the knowledge of simple materials to model more complicated systems, learning with limited data or incomplete labels, identifying meaningful spectra and materials representations, mitigating spectral noise, and others. We present an outlook on a few emerging roles machine learning may play in broad types of scattering and spectroscopic problems in the foreseeable future.

Published under an exclusive license by AIP Publishing. https://doi.org/10.1063/5.0049111

#### **TABLE OF CONTENTS** 3. Autoencoder and generator ..... 5 I. INTRODUCTION ..... 4. Graph neural networks ..... 6 A. Neutron and x-ray scattering in the data era. . . . . 2 5. Nonparametric learning algorithms..... 6 II. STATIC PROPERTIES IN RECIPROCAL OR REAL B. Integrating machine learning into the scattering 2 SPACE..... setup ..... 6 C. Machine learning architectures for scattering A. Diffraction with machine learning..... 4 1. Diffraction or structure as input, property as output..... 1. Representation of materials..... 2. Representation of scattering data..... 7 2. Diffraction as input, structure as output . . . .

Quantum Matter Group, Massachusetts Institute of Technology, Cambridge, Massachusetts 02139, USA

<sup>&</sup>lt;sup>2</sup>Department of Mechanical Engineering, Massachusetts Institute of Technology, Cambridge, Massachusetts 02139, USA

<sup>&</sup>lt;sup>3</sup>Department of Materials Science and Engineering, Massachusetts Institute of Technology, Cambridge, Massachusetts 02139, USA

<sup>&</sup>lt;sup>4</sup>Department of Applied Physics, School of Engineering and Applied Sciences, Harvard University, Cambridge, Massachusetts 02138, USA

<sup>&</sup>lt;sup>5</sup>Department of Nuclear Science and Engineering, Massachusetts Institute of Technology, Cambridge, Massachusetts 02139, USA

<sup>&</sup>lt;sup>6</sup>Fritz Haber Institute, Max Planck Society, 14195 Berlin, Germany

<sup>&</sup>lt;sup>7</sup>Computational Research Division and Center for Advanced Mathematics for Energy Research Application, Lawrence Berkeley National Laboratory, Berkeley, California 94720, USA

<sup>&</sup>lt;sup>8</sup>Department of Physics and Astronomy, Clemson University, Clemson, South Carolina 29634, USA

Neutron Scattering Division, Oak Ridge National Laboratory, Oak Ridge, Tennessee 37831, USA

<sup>&</sup>lt;sup>10</sup>Center for Nanoscale Materials, Argonne National Laboratory, Lemont, Illinois 60439, USA

<sup>&</sup>lt;sup>a)</sup>Author to whom correspondence should be addressed: mingda@mit.edu

	3. Unsupervised learning for diffraction data
В.	Small-angle neutron and x-ray scattering
	1. Spectra as input, structure as output
	2. Spectra as input, other property as output
C.	Imaging and tomography
	CTROSCOPIES AND DYNAMICAL
PRC	PERTIES
	X-ray absorption spectroscopy
	Photoemission spectroscopies
C.	Inelastic scattering
	ERIMENTAL INFRASTRUCTURE AND DATA 1
A.	Instrument and beam
В.	Data collection and processing
V. OUTLOOK	
A.	Machine learning on time-resolved
	spectroscopies
В.	Leveraging information in real and reciprocal
	spaces 1
C.	Multimodal machine learning
D.	High-performance computing for quantum
	materials
E.	Conclusion: Fundamental impact on
	experimental facilities

#### I. INTRODUCTION

#### A. Neutron and x-ray scattering in the data era

Neutron and x-ray scattering are two closely related and complementary techniques that can be used to measure a wide variety of materials structural and dynamical properties from atomic to mesoscopic scales.<sup>1,2</sup> Representing two state-of-the-art materials characterization techniques, neutron and x-ray scattering have undergone significant advancement in the past several decades. While the average neutron flux for reactor-based neutron generation has reached a plateau of  $\sim 10^{15}$  n/cm<sup>2</sup>/s, accelerator-based neutron generation has improved steadily over the past 50 years<sup>3</sup> [Fig. 1(a)]. The planned Second Target Station (STS) at Oak Ridge National Lab (ORNL) is expected to reach 25 times enhancement in brightness and a factor of 10-1000 capability enhancement in instruments compared to other neutron sources in the United States. For x-ray scattering, the peak brightness of synchrotron sources has increased drastically across a broad range of x-ray photon energies<sup>4</sup> [Fig. 1(b)]. In fact, the improvement in peak brightness of synchrotron x-ray sources even exceeds the rate of Moore's law<sup>5,6</sup> [Fig. 1(c)], with a few major facility upgrades, such as Advanced Photon Source-Upgrade (APS-U), European Synchrotron Radiation Facility-Extremely Brilliant Source (ESRF-EBS), and Positron-Electron Tandem Ring Accelerator (PETRA-IV), bringing significant capability boosts. A direct consequence of the enhanced capability is the high efficiency of data collection, enabling the measurement of more diverse types of materials.

In addition to increased data availability for a broader materials composition space, the higher brightness further opens up the possibility for higher-dimensional data collection for a single material type or within one scattering experiment. Spectroscopies, like time-of-flight inelastic neutron scattering, measure the dynamical structure factor in four-dimensional (4D) momentum–energy  $(\mathbf{Q},\omega)$  space, while x-ray photon correlation spectroscopy measures the intensity auto-

correlation in 4D momentum—time  $(\mathbf{Q},t)$  space. The emerging frontier of multimodal scattering, which simultaneously measures samples with multiple probes, or in *in situ* environments such as extreme temperatures or pressures, elastic strain, or applied electrical and magnetic fields, introduces additional dimensions to the measured parameter space. Alongside high intrinsic momentum  $\mathbf{Q}$ , energy  $\omega$ , and time t dimensions, multimodality leads to an even higher overall data dimension and adds inevitable complexities to data analysis.

Finally, the discovery of new functional and quantum materials—often accompanied by novel or unexpected emergent properties—poses a significant challenge to materials analysis. In many scattering experiments with a given measurable signal  $S_{\rm exp}\left(\mathbf{Q},\omega,t,\ldots\right)$ , associated theoretical models  $S_{\rm model}(\mathbf{Q},\omega,t,\ldots;\boldsymbol{\theta})$  exist, parameterized by a set of fitting parameters  $\{\boldsymbol{\theta}\}$  representing materials properties to extract. For the optimal fitting parameters  $\boldsymbol{\theta}=\boldsymbol{\theta}_{op}$ , the difference between the experiment  $S_{\rm exp}$  and model  $S_{\rm model}$  reaches a minimum, i.e.,

$$\mathbf{\theta}_{op} = \arg\min_{\mathbf{\theta}} \|S_{\exp}(\mathbf{Q}, \omega, t, ...) - S_{\text{model}}(\mathbf{Q}, \omega, t, ...; \mathbf{\theta})\|.$$

However, even for a perfect fit  $S_{\exp}(\mathbf{Q},\omega,t,\ldots) \equiv S_{\mathrm{model}}(\mathbf{Q},\omega,t,\ldots;\boldsymbol{\theta}_{op})$ , the information that can be extracted is still ultimately limited by the theoretical model itself. Until recently, avenues that can access materials properties outside the parameter set  $\{\boldsymbol{\theta}\}$  have been lacking.

In short, large data volume, high data dimension combined with multimodality, and new classes of quantum and functional materials with emergent properties that go beyond approximate models all call for a revolutionary approach to learn materials properties from neutron and x-ray scattering data. Machine learning,8 especially emerging techniques that incorporate physical insight 10-15 or respect symmetries and physical constraints of atomic, crystalline, and molecular structures, 16-26 appears to be a promising and powerful tool to extract useful information from large, high-dimensional experimental datasets,<sup>27</sup> going far beyond approximate analytical fitting models. The past few years have witnessed a surge in machine learning research with scattering and spectroscopic applications. Even so, we foresee that machine learning, if properly implemented, has the potential not only to serve as a powerful tool to conduct data analysis but also to gain new knowledge and physical insight from materials, which can assist experimental design and accelerate materials discovery.

### B. Integrating machine learning into the scattering setup

Machine learning has already been widely applied to materials science in many areas, especially in directly predicting or facilitating predictions of various materials properties from structural information, including but not limited to mechanical properties, <sup>24,26,28,29</sup> thermodynamic properties, <sup>28,30–32</sup> and electronic properties. <sup>24,33–39</sup> Their strong predictive power and capacity for representation learning enable machine learning models to perform comparably to more expensive numerical models, like first-principles calculations, at much lower computational cost. This asset greatly accelerates materials discovery and design. <sup>40–45</sup> Machine learning models can also distill complex structural information <sup>46–48</sup> and be trained to acquire interatomic force fields and potential energy surfaces, <sup>49–54</sup> where the accurate, yet computationally cheap access to atomic potentials has proven

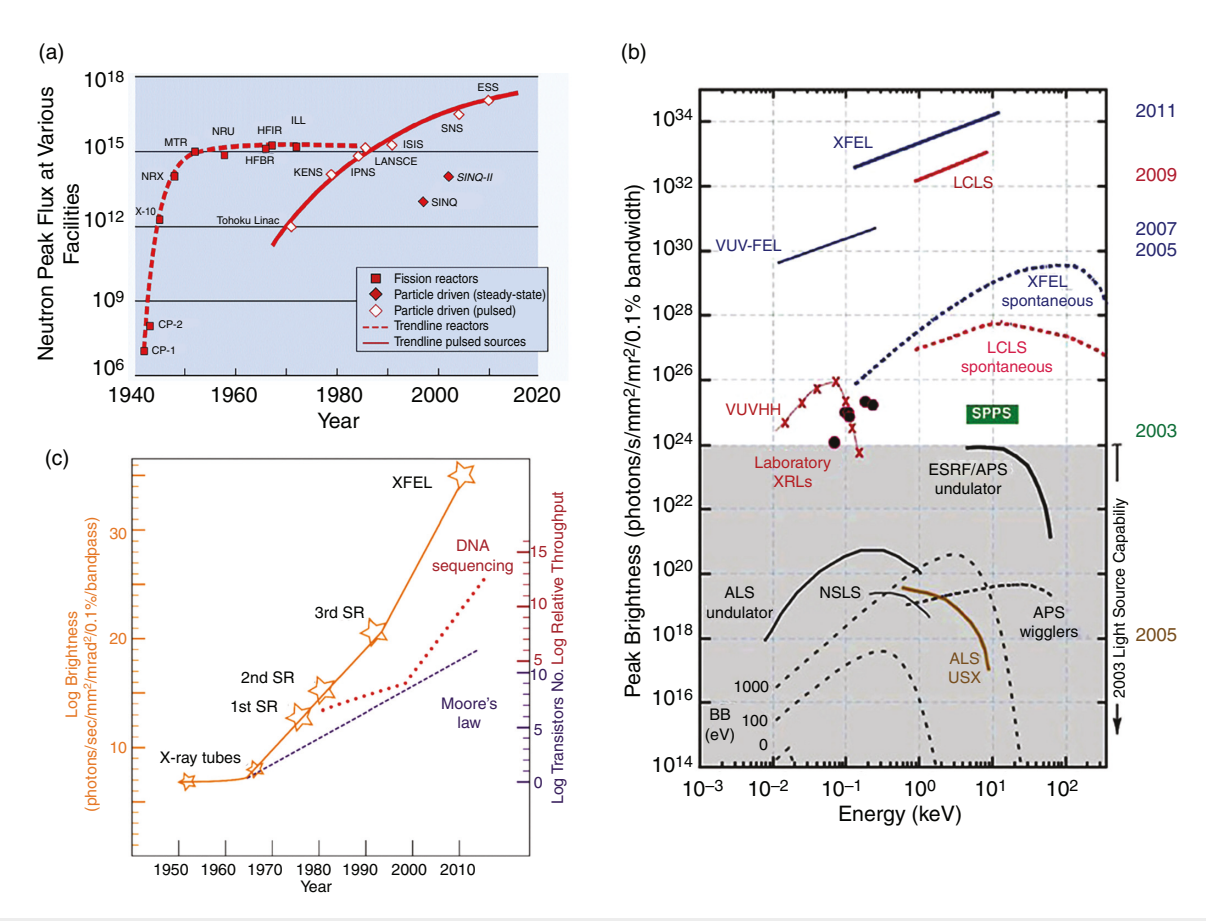


FIG. 1. Neutron and x-ray scattering in the data era. (a) Improvement of neutron flux in reactor-based neutron generation (dashed line) and accelerator-based spallation neutron generation (solid line). Reprinted with permission from Bohn et al., ESS Project 1 (2002). Copyright 2002 European Spallation Source. (b) Drastic enhancement of peak brightness in x-ray scattering at various energy scales. Reprinted with permission from U.S. National Research Council, Committee on Atomic Molecular and Optical Sciences. Copyright 2007 National Academies Press. (c) Comparison of increasing speed of peak brightness of synchrotron x-ray scattering and the Moore's law of microelectronics. Reprinted with permission from Su et al., Crystallogr. Rev. 21, 122–153 (2015). Copyright 2014 Taylor & Francis Group. BB, broadband; CP-1, Chicago Pile 1; HFBR, High Flux Beam Reactor; HFIR, High Flux Isotope Reactor; ILL, Institut Laue—Langevin; IPNS, Intense Pulsed Neutron Source; ISIS, International Science Information Service; KENS, National Laboratory for High Energy Physics Neutron Source; LANSCE, Los Alamos Neutron Science Center; Linac Coherent Light Source (LCLS), linear coherent light source; MTR, Materials Test Reactor; NRU, National Research Universal; NRX, Nuclear Rocket Experiment; SINQ, Swiss Spallation Source; SNS, Spallation Neutron Source; SPPS, solid phase peptide synthesis; VUV-FEL, vacuum ultraviolet free-electron laser; VUVHH, vacuum ultraviolet hybrid heterostructure; X-10, Nuclear Reactor Class 10; XFEL, x-ray free-electron laser.

successful in simulating the transitions in a disordered silicon system with  $100\,000$  atoms. Evidently, machine learning models have already initiated a paradigm shift in the way people study materials science and physics.  $^{56-62}$ 

To see how machine learning can be applied to neutron and x-ray scattering, we show a simple scattering setup in Fig. 2(a). A beam of neutrons or x-ray photons is generated at the source. After passing through the beam optics that prepares the incident beam state, the beam impinges on the sample with a set of incident parameters  $(I_i, \mathbf{k}_i, E_i, \varepsilon_i, \ldots)$ , where  $I_i, \mathbf{k}_i, E_i$ , and  $\varepsilon_i$  denote the incident beam intensity, momentum, energy, and polarization, respectively. After interacting with the sample, the scattered beam can be described by another set of parameters  $(I_s, \mathbf{k}_s, E_s, \varepsilon_s, \ldots)$ , which are partially or fully recorded by the detector. In this source–sample-detector tripartite scheme, the possible application scope of machine learning can be seen clearly: At the "source" stage,

machine learning can be used to optimize beam optics; at the "sample" stage, to better learn materials properties; and at the "detector" stage, to improve data quality, such as realizing superresolution. Setting aside the source and detector stages, which will be introduced in Sec. IV, we focus first on the sample stage, particularly the application of machine learning to relate materials spectra and their properties.

To further illustrate the general relationship between machine learning and scattering experiments, we consider the scattering data as one component in a typical machine learning architecture. In the case of supervised machine learning, the scattering or spectral data can serve either as input to predict other materials properties [Fig. 2(b)] or as output generated from known or accessible materials parameters, such as atomic structures and other materials representations [Fig. 2(c)]. Alternately, unsupervised machine learning can be used to identify underlying patterns in spectral data through dimensionality

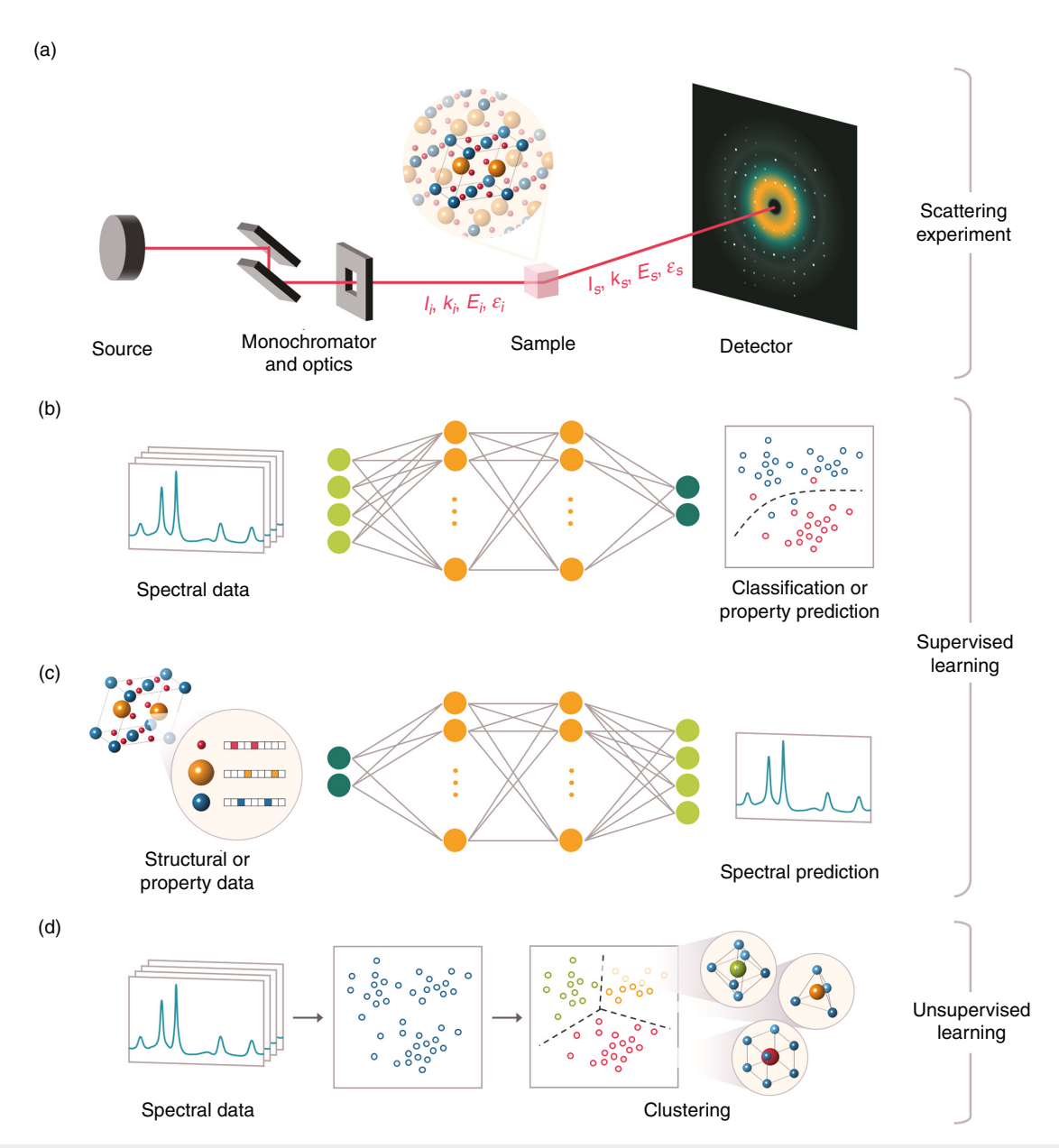


FIG. 2. Machine learning in a neutron and x-ray scattering pipeline. (a) Schematic of a typical scattering setup. (b) Spectral data serving as input to a supervised machine learning model for a materials' classification or property prediction task. (c) Materials structural or property data serving as input to a supervised machine learning model for direct and efficient prediction of the full scattering spectra. (d) Spectral data as part of an unsupervised machine learning task that can identify inherent patterns or clusters within the dataset that may correspond to meaningful physical parameters.

reduction and clustering, which can be useful for data exploration or identification of key descriptors in the data [Fig. 2(d)].

#### C. Machine learning architectures for scattering data

With the various roles machine learning may play in a scattering experiment pipeline, one may ask what particular machine learning architecture should be used for a certain task. Given the no free lunch theorem for optimization, 63 many algorithms are interchangeable.

Even so, a number of machine learning models are naturally suited to scattering experiments. Here, we introduce a few categories of useful architectures, many of which are implemented in the examples that will be discussed Secs. II–IV.

#### 1. Representation of materials

For materials studies, the representation of materials, particularly atomistic structures, is crucial. Various representational approaches

have been developed to describe molecules and solids. These methods include the Coulomb matrix representation, <sup>64</sup> which translates molecules into matrices; the Ewald sum matrix representation, which generalizes the Coulomb matrix to periodic structures; <sup>65</sup> the partial radial distribution function (PRDF), which describes the radial density of species surrounding an atom; <sup>16</sup> atom-centered symmetry functions, which capture both radial and angular information; <sup>66</sup> and the power spectrum defined by the Smooth Overlap of Atomic Positions (SOAP) descriptor. <sup>67</sup> An excellent review of different materials representations can be found in Schmidt *et al.* <sup>58</sup>

#### 2. Representation of scattering data

Complementary to materials representation is that of scattering data. The scattering intensity can be represented as a high-dimensional array,  $I \in \mathbb{R}^{N_{\mathbf{k}} \times N_{\omega} \times N_{\varepsilon}}$ , indexed by momentum  $\mathbf{k}$ , energy  $\omega$ , and polarization  $\varepsilon$ . Such data structures are naturally compatible with convolutional neural networks (CNNs), which are widely applied in image processing. Atomic structures can also be interpreted as images by regarding them as density fields based on atomic species and positions on 3D real-space grids, which enables them to work with convolutional filters. 44,68 Architectures beyond CNNs, such as deep U-Nets, are also widely used to compress the feature size while

increasing the number of features, with skip connections to corresponding layers<sup>69</sup> [Fig. 3(a)].

#### 3. Autoencoder and generator

Another powerful architecture is the variational autoencoder (VAE),<sup>70</sup> which compresses the input into a distributed area in a lower-dimensional latent space (encoding) then reconstructs the input from this low-dimensional representation (decoding). The latent space is thus a "compressed" continuous representation of the training samples, which can be an effective strategy for learning meaningful, continuous representations of materials properties [Fig. 3(b)]. For example, VAEs can be combined with CNNs to learn latent representations of atomic structures.<sup>68</sup> Moreover, the stability of crystal structures can be easily inferred from latent space clustering,<sup>44</sup> and similar methods can also be applied to analyze scattering data, such as x-ray absorption spectroscopy (XAS)<sup>39</sup> or neutron diffuse scattering.<sup>7</sup> Another use of VAE is to serve as a generative model to facilitate materials design, such as generating new structures through sampling and exploring the latent space. 44 The generative adversarial network (GAN) is another popular generative framework that is composed of a generator and a discriminator<sup>72</sup> [Fig. 3(c)]. The generator is a neural network that converts latent space representations to desired objects,

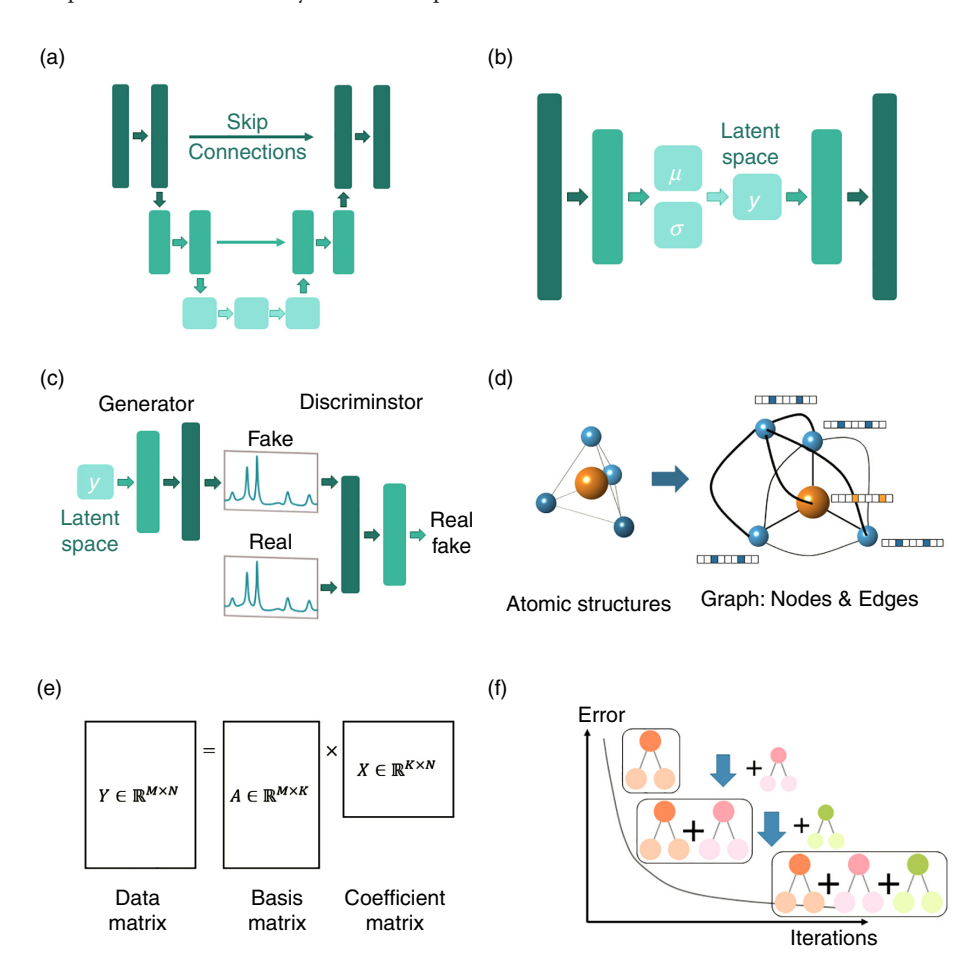


FIG. 3. Common machine learning architectures. (a) U-Net architecture. (b) Variational autoencoder (VAE). (c) Generative adversarial network (GAN). (d) Crystal graph convolutional neural network (CGCNN). (e) Non-negative matrix factorization (NMF). (f) Gradient boosting trees (GB Trees).

such as crystal structures,<sup>45</sup> while the discriminator is a second network that aims to discern "fake" (generated) from "realistic" (training) samples. The main goal of the generator is to create high-fidelity objects that can effectively fool the discriminator, thereby generating outputs that closely resemble real data.

#### 4. Graph neural networks

Graph neural networks with nodes and edges are naturally suited to represent atomic structures, where atoms can be represented as nodes and bonds as edges in a graph. In graphs, information at each node is updated using information from its neighboring nodes, mimicking a local chemical environment in which an atom is most influenced by its neighboring atoms. Crystal graph CNNs<sup>24</sup> [Fig. 3(d)] and Euclidean neural networks (E<sup>3</sup>NN)<sup>19,73,74</sup> are two such examples. E<sup>3</sup>NNs are equipped with sophisticated filters that incorporate radial functions and spherical harmonics, which render these networks equivariant to 3D Euclidean transformations; thus, all crystallographic symmetries of input structures are preserved. Because symmetry is built into these models, E<sup>3</sup>NNs do not require data augmentation and can achieve accurate results without significant data volume.

#### 5. Nonparametric learning algorithms

The aforementioned machine learning architectures contain parameters that need to be learned during the training process, yet plenty of unsupervised learning or nonparametric algorithms exist that do not contain learnable parameters but are more procedural. For instance, k-means clustering and Gaussian mixture models (GMMs) can be applied to data clustering; decision trees, such as gradient boosted trees (GB Trees), can be used for classification and regression [Fig. 3(f)]; and principal component analysis (PCA) can be used for dimensionality reduction. One particularly interesting method is nonnegative matrix factorization (NMF), which decomposes a matrix into lower dimensions but maintains an intuitive representation 75,76 [Fig. 3(e)]. Conceptually, NMF resembles the widely used dimension reduction algorithm of PCA but with additional non-negativity constraints. Such non-negative matrix descriptions are extremely powerful when interpreting certain physical signals, such as music spectrograms. Likewise, scattering data collected from detectors have non-negative counts in the array  $I \in \mathbb{R}^{N_k \times N_\omega \times N_\varepsilon}$  and can, in principle, be decomposed with NMF.

### II. STATIC PROPERTIES IN RECIPROCAL OR REAL SPACE

#### A. Diffraction with machine learning

To see how machine learning can benefit neutron and x-ray diffraction (XRD), we follow the taxonomy illustrated in Fig. 2. In a supervised learning problem, diffraction signatures can serve as an input to predict either materials structure or properties, while in an unsupervised learning approach, clustering of diffraction data can be used to infer patterns or relationships between materials in the absence of known data labels. The inverse problem, such as using structures or other physical properties to predict diffraction patterns, can either be posed as physics-based forward problems or are less relevant to machine learning studies and will be left out of this discussion.

#### 1. Diffraction or structure as input, property as output

Since the most straightforward information one can extract from diffraction data is atomic structure, whose variation is directly associated with mechanical properties, we start by discussing high-entropy alloys as an example to show how diffraction can be used to predict elastic constants in complicated materials. High-entropy alloys have received tremendous attention in the past decade due to their extraordinary strength-to-weight ratios and chemical stability. However, given their complex atomic configurations, direct property calculation has been challenging. To enable efficient prediction of elastic constants in high-entropy alloys, Kim et al. conducted a combined neutron diffraction, ab initio calculation, and machine learning study.<sup>78</sup> In this study, an in situ diffraction experiment and high-quality ab initio density functional theory (DFT) calculations with special quasi-random structure (SQS) were carried out on the high-entropy alloy Al<sub>0.3</sub>CoCrFeNi. The experimental result and ab initio calculations of elastic constants showed good agreement and, thus, can serve as the ground truth values [Fig. 4(a), ground truth block]. Due to the limited neutron beamtime and high computational cost of DFT + SQS, it would be unrealistic to either measure or compute the elastic constants in a large number of high-entropy alloys. To bridge this gap, the authors built a GB Tree-based predictive model using a separate set of nearly 7000 ordered, crystalline solids from the Materials Project, in which the elastic constants have already been properly labeled [Fig. 4(a), machine learning block]. It is worth mentioning that the training set and validation set do not contain any high-entropy alloys. Even so, there are a few indicators that demonstrate the model's transferability and generalizability. On the one hand, the elastic constants of Al<sub>0.3</sub>CoCrFeNi predicted by the machine learning model show good agreement with ground truth values established by experiments and DFT + SQS calculations. On the other hand, the lower training error compared to a benchmark model, and the reasonable dependence as a function of training data volume, give a level of confidence in the model generalizability.

The high-entropy alloy example demonstrates a general pathway for efficient property predictions in complex materials, where data scarcity is a common challenge. With a small labeled "hard" dataset  $\{x_i^H, y_i^H\}, i = 1, 2, ..., n$  that is difficult to acquire, training a machine learning model directly may not be feasible due to the low data volume n. To make machine learning possible, a different, large set  $\{x_i^E, y_i^E\}$ , with j = 1, 2, ..., N and  $N \gg n$ , can be used, where the features  $x_i^E$  and labels  $y_i^E$  are easier to obtain, such as properties of simple crystalline solids or outputs of efficient forward computations. The key step is to build a predictive model using the large, "easy" set  $\{x_i^E, y_i^E\}$ that also minimizes the test error from  $\{x_i^H, y_i^H\}$  [Fig. 4(b)]. A few approaches can help to achieve this step, such as transfer learning, where the learning task in one setting (e.g., easy set) is generalized and transferred to another setting (e.g., hard set), and similar examples will be discussed frequently in Secs. II-IV. The outcome thus has a level of generalizability. In the previous example,

 $x^H = diffraction/structure in high entropy alloys,$ 

 $y^{H} = elastic constants in high entropy alloys,$ 

 $x^E = structure in crystalline solids,$ 

 $y^E = elastic constants in crystalline solids,$ 

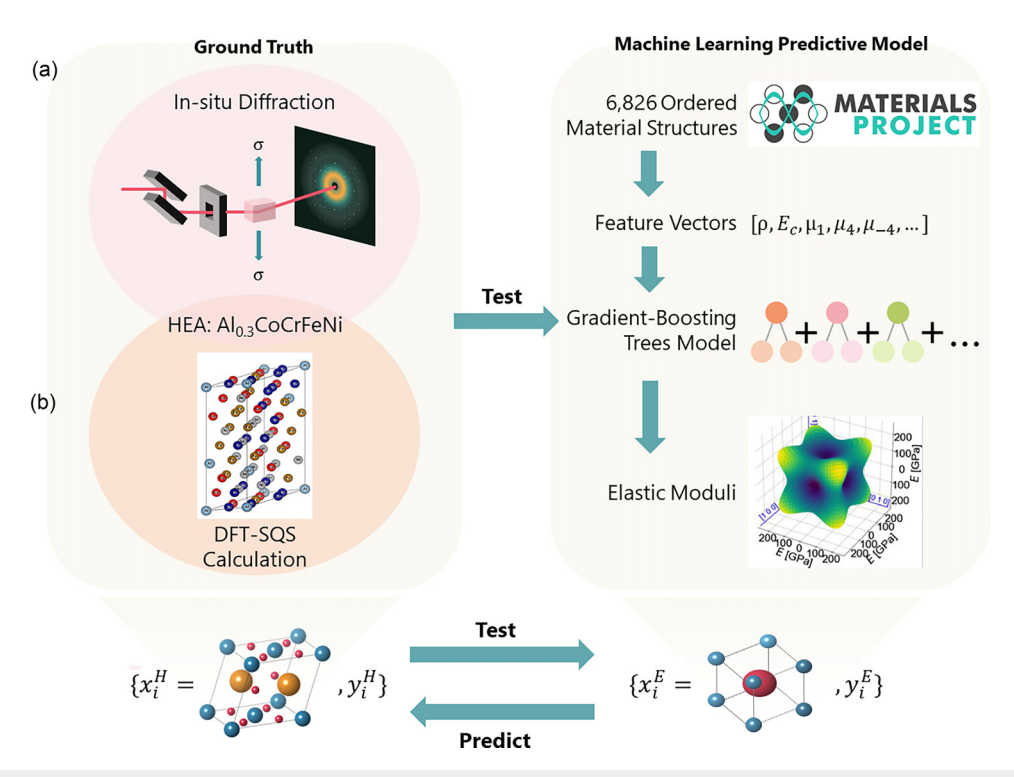


**FIG. 4.** Machine learning models for predicting properties that are hard to acquire. (a) Predicting elastic moduli of high-entropy alloys (HEAs) using the machine learning–based model that is trained with ordered crystalline solids. Reprinted with permission from Kim *et al.*, Acta Materialia **181**, 124–138 (2019). Copyright 2019 Elsevier.<sup>78</sup> (b) Machine learning models can be trained with data that are from or augmented by easily accessible samples; then the models can be used to predict properties that are hard to acquire.

and  $\{x_i^H, y_i^H\}$  is simply used to test the machine learning model built upon  $\{x_j^E, y_j^E\}$  [Fig. 4(b), right-facing arrow].

#### 2. Diffraction as input, structure as output

In addition to the direct structure-to-property prediction, given the close relationship between diffraction and structure, another central machine learning application is diffraction-to-structure prediction, as done by Garcia-Cardona *et al.* for neutron diffraction.<sup>79</sup> The conventional solution to this problem is iterative optimization of computed scattering patterns from physics-based forward models. A key challenge, however, lies in the scarcity of labeled neutron diffraction data, i.e.,

$$x^{H} = experimental neutron diffraction,$$
  
 $y^{H} = y^{E} = atomic structure.$ 

To facilitate training of machine learning models, simulated diffraction patterns  $x^E = simulated neutron diffraction$  may be generated by sweeping the structure parameter space (comprising lattice parameters, unit cell angles, etc.), which relies on data augmentation [Fig. 4(b), left-facing arrow]. Similarly, augmented XRD data can be used to obtain crystal dimensionality and space group information. Another approach is to use the atomic pair distribution function (PDF) to

predict space group information.  $^{81}$  Conventionally, the PDF is a powerful tool in determining local order and disorder information.  $^{82}$  By setting

$$x^{E} = simulated PDF,$$
  
 $y^{E} = y^{H} = space group,$ 

PDF may further be exploited to allow determination of global space group information. A separate set,  $x_i^H =$  experimental PDF, containing 15 examples is used as a test dataset [Fig. 4(b), right-facing arrow], where the space groups of 12 examples are among the top six predicted labels.

#### 3. Unsupervised learning for diffraction data

In addition to supervised learning on XRD and PDF spectra, unsupervised learning, which aims to elicit the internal categorical structure of data, can also assist the analysis and interpretation of scattering measurements. Since mature fitting and refinement methods exist to identify phases among different crystallographic structures, one key application for unsupervised learning is phase identification in a complex compositional phase space where multiple phases coexist. One major success of unsupervised learning in the context of XRD analysis has been the use of NMF and its variants, <sup>83</sup> which can decompose diffraction spectra into simpler basis patterns. Recalling the

introduction in Sec. I.C, NMF decomposes a non-negative matrix  $Y \in \mathbb{R}^{M \times N}$  into two smaller non-negative matrices, namely, the basis matrix  $A \in \mathbb{R}^{M \times K}$ , representing K basis patterns, and the coefficient matrix  $X \in \mathbb{R}^{K \times N}$ , indicating contributions of those patterns. In XRD,  $Y_{mn}$  denotes the diffraction intensity of the mth composition at the nth sample diffraction angle (or, equivalently, the momentum transfer Q). Long et al. applied NMF to identify phases within the metallic Fe–Ga–Pd ternary compositional phase diagram. <sup>84</sup> For

instance, given a nominal composition  $Fe_{46}Pd_{26}Ga_{28}$ , NMF decomposes its XRD pattern [Fig. 5(a), middle] into a weighted sum of five basis patterns [Fig. 5(a), bottom and top] with a total number of  $K_{\rm NMF}=9$  basis patterns. The entire structural phase diagram in the compositional phase space can then be constructed [Fig. 5(b)] and contains the quantitative weight information of each pure constituent phase. Limitations exist, however, when the same nominal composition corresponds to different structural combinations with slightly

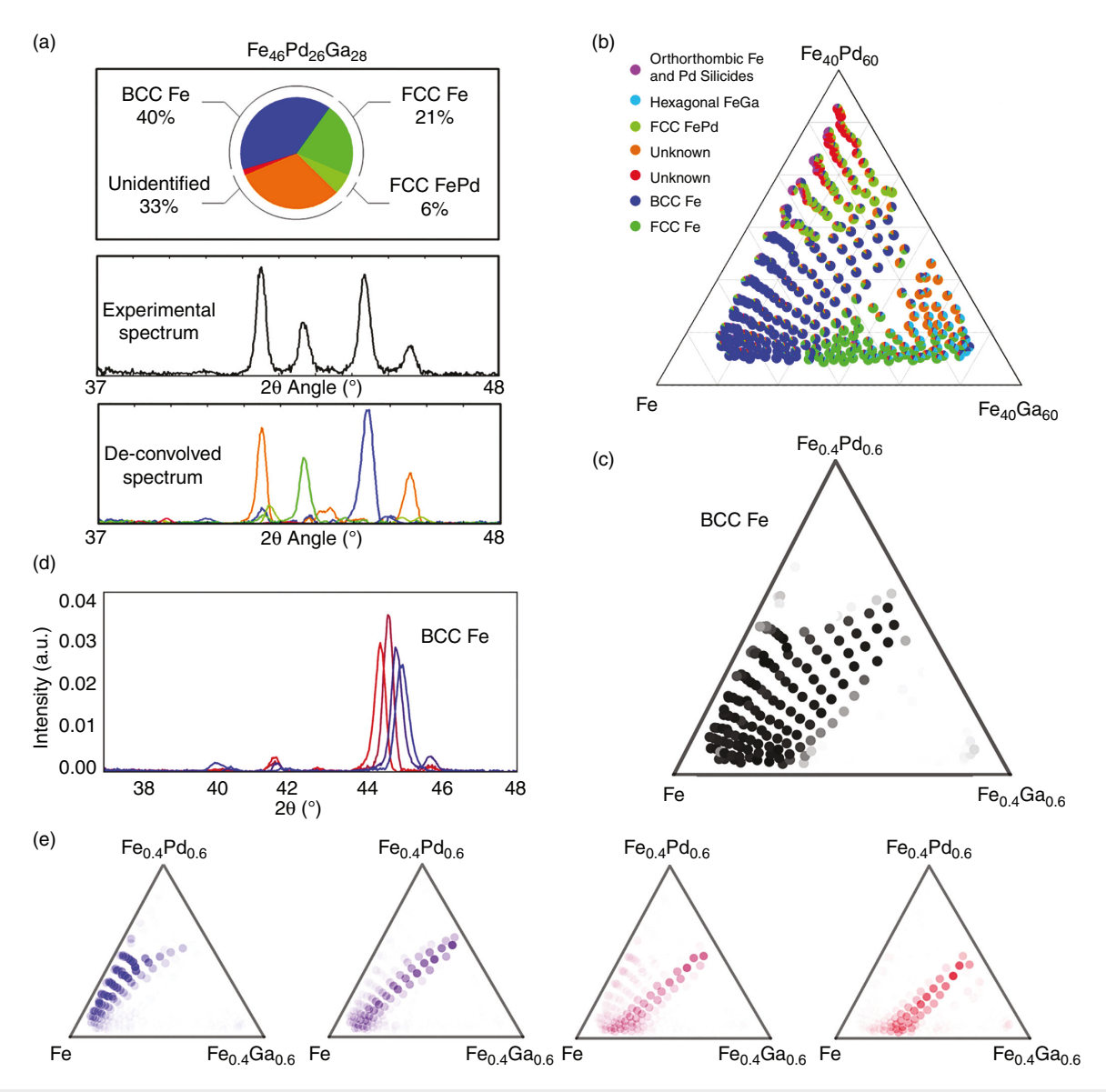


FIG. 5. Structural phase mapping of x-ray diffraction data with non-negative matrix factorization (NMF). (a) Weights of the basis patterns for Fe<sub>46</sub>Pd<sub>26</sub>Ga<sub>28</sub> (top) and decomposition of the experimental XRD spectrum (middle) into the weighted basis patterns (bottom). (b) Structural phase diagram of the Fe–Ga–Pd system constructed using the weights of the basis diffraction patterns found by NMF. Reprinted with permission from Long *et al.*, Rev. Sci. Instrum. **80**, 103902 (2009). Copyright 2009 AIP Publishing. (c) Structural phase diagram of the Fe–Ga–Pd system reconstructed using NMF with custom clustering (NMFk). (d) Four basis patterns of the Fe–Ga–Pd system obtained by NMFk representing the BCC Fe phase, which differ only in peak shift. (e) The weight of each basis pattern from (d) drawn in the corresponding color, showing the peak evolution in the composition phase space. Reprinted with permission from Stanev *et al.*, npj Comput. Mater. **4**, 43 (2018). Licensed under a Creative Commons Attribution (CC BY) license. (CC BY) license. (CC BY) license.

varied diffraction peaks. To overcome this limitation, Stanev et al. extended NMF with custom clustering (NMFk) algorithms to capture the nuanced peak shifts from changes in the lattice constant, which can further resolve the constituent phases, even within the same nominal composition. 85 Compared to NMF, where the small matrix dimension K is chosen manually through trial and error, NMFk automatically searches and optimizes K. The same Fe-Ga-Pd dataset first analyzed in Long et al.84 by NMF is re-analyzed using NMFk.85 An optimized basis pattern number  $K_{\text{NMF}} = 13$  is found by NMFk, which contains four basis patterns representing BCC Fe structures but with a slight peak shift [Fig. 5(d)]. Although the BCC Fe structure corresponds to almost identical regions in the structural phase diagrams produced by NMFk and NMF methods [comparing Fig. 5(c) to blue points in Fig. 5(b)], the weight of each NMFk basis pattern for the BCC Fe structures can be seen clearly [Fig. 5(e)], tracing the nuanced lattice parameter change in the phase diagram. In a more recent example, XRD measurements were also analyzed to obtain quantum phase diagrams with charge ordering and structural phase transitions using a novel approach called XRD temperature clustering (X-TEC), which builds upon the GMM.8

Beyond learning materials properties and identifying structure-property relationships, machine learning has also been applied to empower the analysis of diffraction patterns themselves<sup>87–91</sup> or to automate the structure refinement process. <sup>92</sup> Since the focus here is to explore materials properties, we leave those examples to Sec. IV B as part of the section on the data analysis process.

#### B. Small-angle neutron and x-ray scattering

Small-angle scattering (SAS), which includes small-angle neutron scattering (SANS) and small-angle x-ray scattering (SAXS), is a powerful technique used to probe structures and their evolution on length scales of 0.5-100 nm. 93,94 They have been widely applied to study soft matter systems, such as rough surfaces, 95 colloids, and polymers, 9 and biological macromolecules, 98-101 as well as mesoscopic magnetic structures, namely, magnetic vortex lattices in superconductors (SANS only). 102-105 In the past few years, a surge of machine learning-augmented SAS works has been reported. To6-118 At least two reasons make SAS an ideal technique that can benefit from machine learning. On the one hand, SAS represents one of the rare techniques for which experimental data can be directly and quantitatively compared to theoretical models with minimal postexperimental data processing. This direct data-to-data comparison increases transferability using computationally easy data  $\{x_i^E, y_i^E\}$  to conduct training with high fidelity. On the other hand, SAS allows for highly efficient synthetic data generation, since in many cases, only effective geometrical models at intermediate scales are needed to compute the 1D SAS spectra I(Q). Even in the case of atomistic scale data generation, methods with low computational cost, such as molecular dynamics, Monte Carlo simulations, or micromagnetic simulations, are generally sufficient.

#### 1. Spectra as input, structure as output

Since the original goal of SAS is to learn structural information, we start by introducing one example that predicts structural properties. Franke *et al.* provided such a machine learning–based structure predictor in biomacromolecular solutions. For a given geometrical object, although the form factor and corresponding SAS spectra are

directly computable [Fig. 6(a)], the effect of disorder must be considered to generate realistic data. To consider this disorder effect, an ensemble optimization method is implemented to generate SAS patterns of random chains, which are averaged to simulate mixtures [Fig. 6(b)] that then augment the original geometrical data. The first task is to classify the shape of macromolecules from SAS. By defining a structural parameter, the radius of gyration  $R_g$ , the original SAS can be compressed onto a 3D parameter space, with the three coordinates representing normalized apparent values V' corresponding to the integral upper bounds of  $|\mathbf{Q}|R_g = 3, 4, 5$ , respectively. It can be seen directly that different basic shapes separate well in this 3D parameter space [Fig. 6(b)]. By performing unsupervised k-nearest neighbor classification, these shapes can also be classified from the SAS curves. To perform a structural parameter prediction, a separate set of atomistic structure data from the Protein Data Bank (PDB) is used to compute both SAS patterns and structural parameters, from which a predictive machine learning model is built, showing good transferability when applied to experimental databases [Fig. 6(c)]. A summarized workflow is shown in Fig. 6(d). In this example, we can still state that

$$x^{H} = experimental SAS,$$
  
 $x^{E} = simulated SAS,$   
 $y^{H} = y^{E} = shape and structural characteristics,$ 

but with two different sources,

 $x^{E1} = geometrically simulated SAS,$  $x^{E2} = atomistically simulated SAS,$ 

depending on whether the target is obtaining shape features or obtaining structural parameters, respectively. Shape classification and structure parameter prediction, with targeted synthetic data augmentation for the respective tasks, represent two key applications of machine learning to SAS, <sup>112,117</sup> and have been employed in studying systems like RNA<sup>114</sup> and 3D protein structures. <sup>116</sup> Machine learning also enables direct analysis using 2D SAS data, <sup>111,118</sup> where traditional analysis methods frequently require data reduction to 1D.

Another example of machine learning in the context of SAS is in micromagnetic structural determination from SANS. As in studies of soft matter, real space structural information is encoded in 2D maps of the neutron scattering cross section. As noted previously, a strong benefit of magnetic SANS is that the structure factor and cross section are relatively straightforward to calculate from a theoretical model—often a micromagnetic continuum model—of the real space magnetization. With sufficiently labeled experimental data and micromagnetic simulations, supervised learning with neural networks or unsupervised clustering methods can be used to solve the inverse scattering problem of determining real space magnetic structures from SANS spectra at the mesoscale.

#### 2. Spectra as input, other property as output

Since the structures of macromolecules are directly linked to their microscopic interactions, one further use of machine learning is to augment SAS to learn interatomic interaction properties. Demerdash *et al.* directly extracted force field parameters from  $SAS^{109}$  using an iterative algorithm as depicted in Fig. 6(e). First, a molecular dynamics (MD) simulation is performed from an initial set of force field

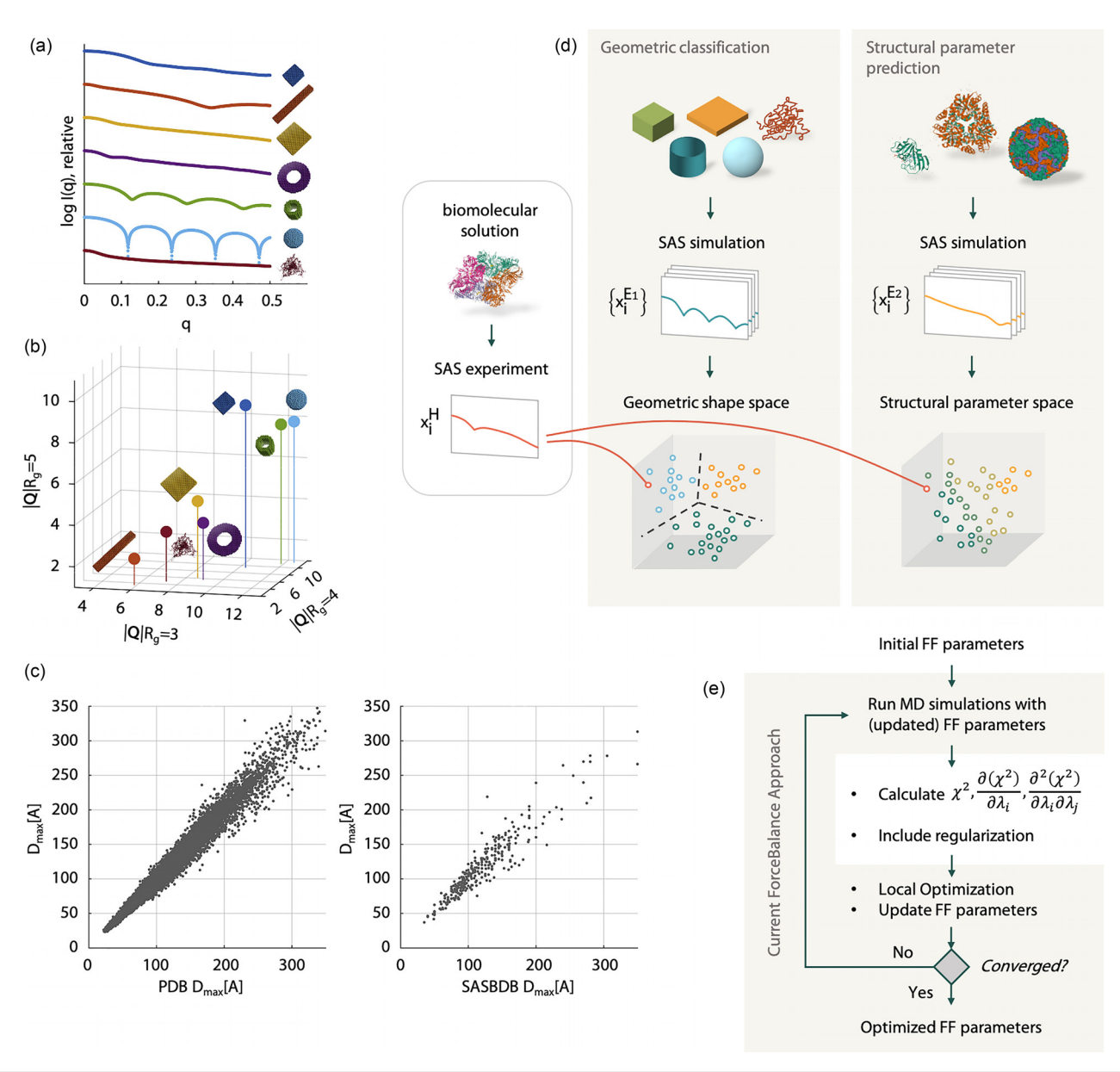


**FIG. 6.** Machine learning for small-angle scattering. (a) Small-angle scattering patterns of geometric objects and a disordered chain. (b) Reduction of each scattering pattern in (a) to three features, corresponding to each axis of the three-dimensional space, and an associated class label. (c) Estimates of the structural parameter  $D_{max}$  for the Protein Data Bank (PDB) dataset (left) and experimental SAS dataset from SAS Biological Data Bank (SASBDB; right) compared to their expected values. (d) Schematic illustration of the workflow followed by Franke *et al.*<sup>108</sup> A model for geometric classification is obtained by reducing the simulated SAS patterns of geometric objects and disordered chains to three features to construct a geometric shape space, with each data point labeled according to its associated geometric class. Similarly, a model for structural parameter prediction is obtained by reducing the simulated SAS patterns of asymmetric units and biological assemblies available in the PDB to the same three features. Each data point in this structural parameter space is associated with a value for each structural parameter of interest, such as maximal extent ( $D_{max}$ ) and molecular mass. Subsequently, the geometry and structural parameters of an entity in an unknown biomolecular solution can be determined by computing the three features using its experimental SAS spectrum, mapping to the corresponding coordinate in either geometric or structural parameter spaces, and weighting the contributions of its k-nearest neighbors. Reprinted with permission from Franke *et al.*, Biophys. J. **114**, 2485–2492 (2018). Copyright 2018 Cell Press. <sup>108</sup> (e) Flowchart depicting the modified ForceBalance-SAS algorithm. Reprinted with permission from Demerdash *et al.*, Front. Mol. Biosci. **6**, 64 (2019). Licensed under a Creative Commons Attribution (CC BY) license. <sup>109</sup> FF, force field.

parameters, and corresponding SAS intensities are then calculated. If the simulated and experimental scattering intensities are in good agreement according to a specified convergence criterion, the current force field parameters are output; otherwise, the parameters

are updated and the process is repeated until optimal force field parameters are obtained. Such refined force field parameters improve the agreement between simulated SAS and experimental data.

#### C. Imaging and tomography

Neutron<sup>119,120</sup> and x-ray<sup>121</sup> imaging encompass a variety of modalities and have become essential techniques to unravel multidimensional and multiscale information in materials systems. As the complexity and size of imaging data grow, machine learning has also been applied to solve a variety of imaging-related computational tasks, including tomography and phase-contrast imaging. Tomography and phase-contrast imaging are two types of high-dimensional imaging techniques sensitive to either the beam absorption or the phase shift associated with sample rotation, respectively. We restrict further discussion to materials science and refer the readers to other reviews for applications in biomedical imaging. Despite the wide variety of imaging modalities used today, the major data processing steps generally include image reconstruction and image segmentation.

In image reconstruction, one recovers the real space information (usually the amplitude and phase of the imaged object) from data obtained at different sample positions. Neural network-based reconstruction algorithms have been shown to improve reconstruction speed and quality, 124 as demonstrated in a neutron tomography experiment.<sup>125</sup> Yang et al. demonstrated the use of a GAN for reconstructing limited-angle tomography data by considering reconstruction as an image translation problem between the sinogram domain and real space. 126 Their method, called GANrec, has been shown to tolerate large missing wedges without obvious degradation in reconstruction quality. GANrec has been successfully applied to tomographic imaging of zeolite particles deposited on a microelectromechanical systems (MEMS) chip, which due to limited rotation capability, has a missing wedge of 110°. The reconstruction from GANrec shows significant improvement over outcomes from conventional reconstruction algorithms, which are corrupted by artifacts due to the missing data.

With regard to image segmentation, in which pixels representing the desired structures are separated from the background, typical approaches include variants of the CNN and U-Net architectures.<sup>59</sup> A number of related studies have been conducted, such as materials defect recognition, <sup>127–129</sup> mineral phase segmentation, <sup>130</sup> automated feature extraction for microtomography, <sup>131</sup> and nondestructive, *in vivo* estimation of plant starch. <sup>132</sup> Deep transfer learning, which has demonstrated great power in image processing, can also be applied to feature extraction in x-ray tomography <sup>133</sup> using a network pretrained on a large image database. Deep U-Nets, on the other hand, are shown to be highly successful on image segmentation tasks. <sup>134</sup>

A particularly powerful technique called coherent diffraction imaging (CDI) has attracted significant research attention since its first demonstration in 1999. 135 Contrary to conventional imaging, the resolution in CDI is not limited by the imaging optics. This allows for 3D structure determination in nanoscale materials through computational phase retrieval. 136,137 Given the data complexity, lack of phase information, and high data volume inherent to this technique, machine learning is becoming a promising tool for CDI analysis. As an example, the shapes of helium nano-droplets have been measured by singleshot CDI with a free-electron laser, where shape classification from the diffraction images could be obtained using a CNN. 131 recently, Cherukara et al. applied the CNN depicted in Fig. 7(a) to directly address the phase retrieval problem in a particular type of CDI called ptychography. 140 By inputting the diffraction patterns at different spatial points of the scan [row A of Fig. 7(b)], the amplitude and phase images of the 2D tungsten calibration chart obtained by the machine learning model [rows C and E of Fig. 7(b)] show good agreement with those retrieved by a conventional iterative phase retrieval algorithm [rows B and D of Fig. 7(b)]. The CNN-assisted approach can effectively speed up scanning by a factor of five, thus greatly reducing the imaging time and dose. Furthermore, Scheinker and Pokharel built an additional model-independent adaptive feedback loop ontop of the CNN output, <sup>141</sup> which allows for more accurate recovery of the 3D shape [Fig. 7(c)]. Iterative projection approaches still demonstrate great flexibility in tomographic reconstruction because constraints such as multiple scattering effects can be captured well by physical models, <sup>142</sup> while they are currently implemented only in a few example cases using machine learning–based approaches in optical imaging. <sup>143</sup>

# III. SPECTROSCOPIES AND DYNAMICAL PROPERTIES A. X-ray absorption spectroscopy

XAS is another characterization technique widely used in materials science, chemistry, biology, and physics. The possibility to reach excellent agreement between experimental and computational data makes XAS suitable for training machine learning models on bulk computational data that translate well to experimental examples. The absorption of x rays reflects electronic transitions from an atomic core orbital to either unoccupied bound levels or the free continuum, producing sharp jumps in the absorption spectrum at specific energies called absorption edges. 144 Such a measurement is therefore sensitive to the species of the absorbing atom as well as to its valence state and local chemical environment, including the local symmetry, coordination number, and bond length. 145,146 As a result, XAS is routinely used in the characterization of materials structural and electronic properties. However, interpretation of XAS spectra ranges from qualitative comparisons with known model complexes, to more quantitative comparisons with theoretical models or band structure calculations, making the process difficult to standardize and automate across different materials and applications. Machine learning methods are therefore sought to better extract and decipher the rich electronic and structural information encoded in XAS signatures. 149 The availability of large XAS databases, such as the XASdb, 150 further facilitates this objective.

To this end, Carbone et al. developed a neural network classifier to identify the local coordination environments of absorbing atoms in >18 000 transition metal oxides using simulated K-edge x-ray absorption near-edge structure (XANES) spectra. 151 The input of their neural network model is the discretized XANES spectrum, while the output is a predicted class label corresponding to one of three coordination geometries: tetrahedral, square pyramidal, and octahedral. The authors achieved an average 86% classification accuracy when using the full (pre-, main-, and post-edge) feature space of the discretized spectra; however, by also training their model using only the pre-edge region, they further revealed the significance of features beyond the pre-edge for accurate classification of the coordination environments [Fig. 8(a)]. The work of Torrisi et al. expanded on this approach by subdividing the discretized XANES spectra into smaller domains ranging from 2.5 to 12.5 eV, thereby capturing spectral features on both coarse and fine scales. 152 The spectrum within each domain is then fit by a cubic polynomial whose coefficients serve as inputs to random forest models for predicting the properties of interest, including coordination number, mean nearest-neighbor distance, and Bader charge. Through this

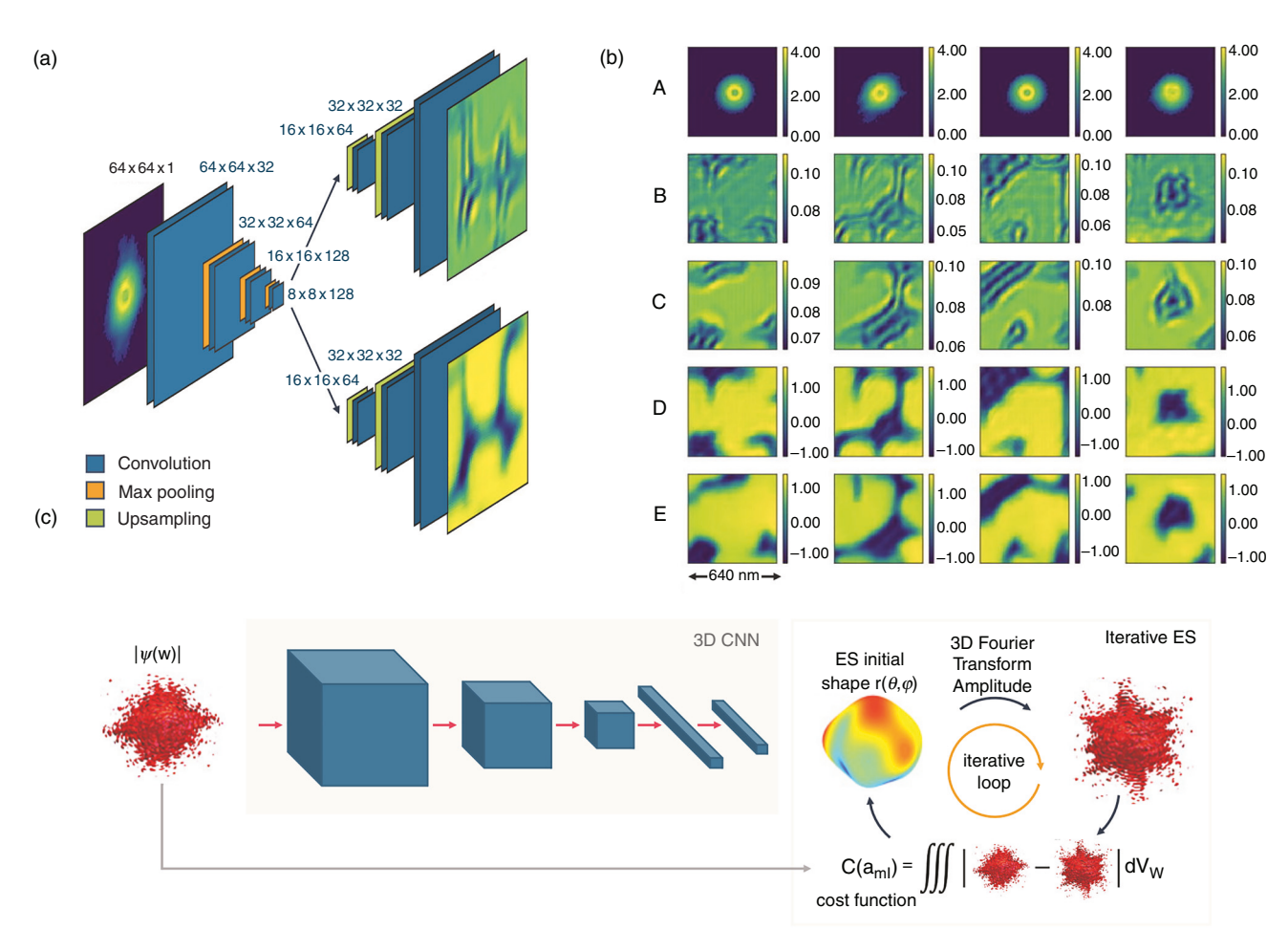


FIG. 7. Machine learning for coherent diffraction imaging. (a) Architecture of PtychoNN, a CNN-based model that directly solves the phase retrieval problem in ptychography. (b) The PtychoNN takes diffraction patterns at different spatial scan points (row A) and retrieve real space amplitude and phase (rows C and E), which show good agreement with the conventional phase retrieval algorithm approach (rows B and D). Reprinted with permission from Cherukara *et al.*, Appl. Phys. Lett. **117**, 044103 (2019). Copyright 2019 AIP Publishing.<sup>140</sup> (c) An adaptive machine learning framework that recovers real space electron densities from diffraction patterns. This framework takes output of the 3D CNN as the initial condition of the extremum-seeking algorithm. Reprinted with permission from Scheinker and Pokharel, J. Appl. Phys. **128**, 184901 (2020). Copyright 2020 AIP Publishing.<sup>141</sup> extremum seeking, expectation sampling.

multiscale featurization, the authors highlighted the importance of developing effective data representations to improve model interpretability and accuracy.

Another focus of machine learning efforts in this context includes accelerating high-throughput modeling of XAS spectra. As a proof of concept, Carbone *et al.* showed that a message-passing neural network (MPNN) is capable of predicting the discretized XANES spectra of molecules to quantitative accuracy by using a graph representation of molecular geometries and their chemical properties. <sup>153</sup> An MPNN, shown in Fig. 8(b), refers to a neural network framework that operates on graph-structured data: Hidden state vectors at each node in the graph are updated according to a function of their neighbors' state vectors for a specified number of time steps, and the results are ultimately aggregated over the entire graph to produce the final output. <sup>154</sup> The structural similarities between MPNNs and molecular systems suggest that

these networks may better predict molecular properties by remaining invariant to the molecular symmetries that help to determine these properties. In their work, Carbone *et al.* constructed each molecular graph by associating with each graph node a list of atom features (absorber, atom type, donor or acceptor states, and hybridization) and with each graph edge a list of bond features (bond type and length). The MPNN then passes the encoded feature information between adjoining nodes to learn effective atomic properties before computing a discretized output XANES spectrum from the final hidden state vectors. The network is optimized by minimizing the mean absolute error between this predicted spectrum and a ground truth XANES spectrum obtained from simulation.

Furthermore, Madkhali *et al.* investigated how the choice of representation for the local environment of an absorbing atom affects the performance of a neural network in predicting the corresponding

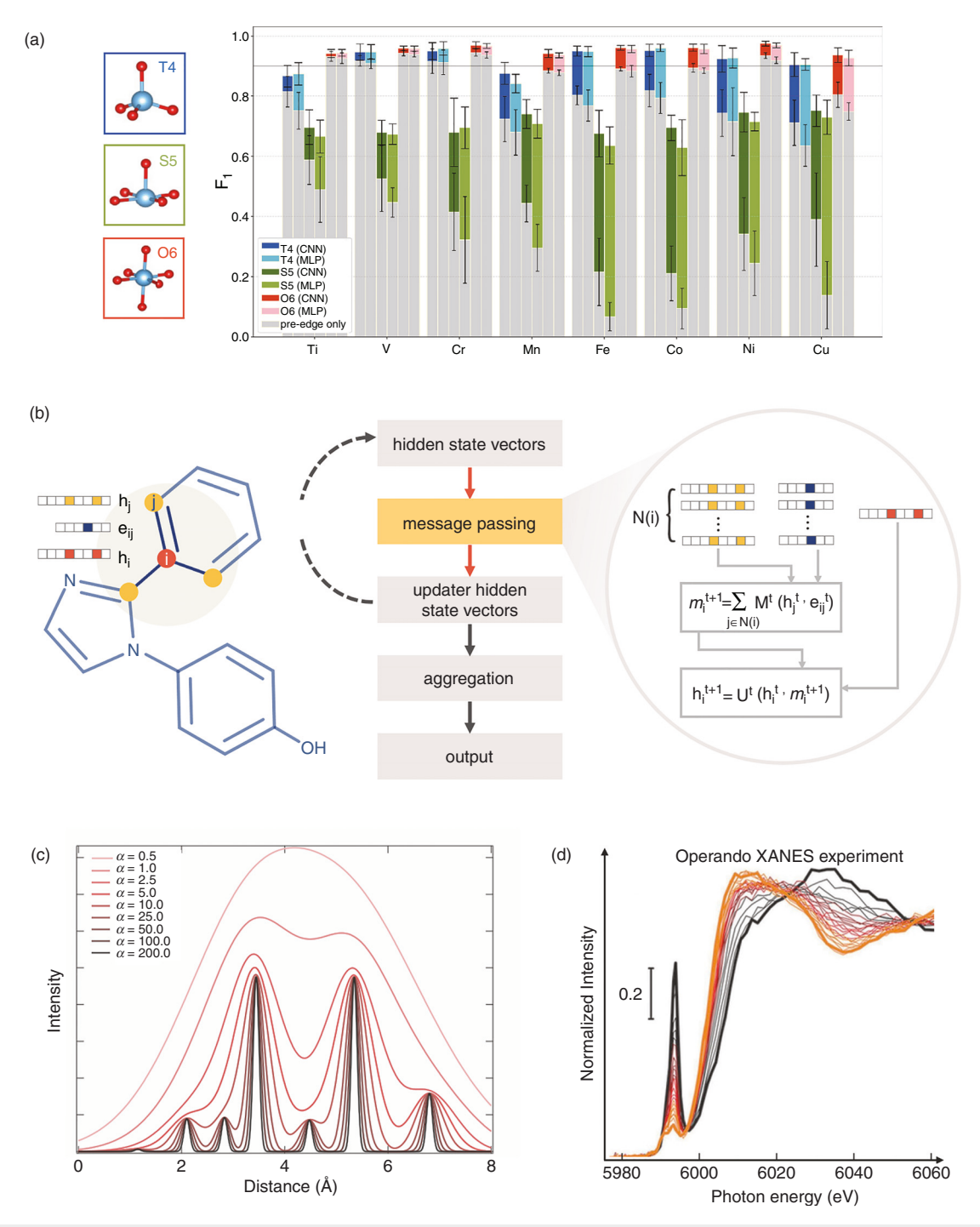


**FIG. 8.** Machine learning for x-ray absorption spectroscopy. (a) F1 scores for the classification accuracy for each coordination environment—tetrahedral (T4), square pyramidal (S5), and octahedral (O6)—depicted at left using two different machine learning models (CNN and multilayer perceptron [MLP]). The full bar height represents the score for models trained on the full XANES feature space, while the gray bars represent the results using only the pre-edge region. Reprinted with permission from Carbone *et al.*, Phys. Rev. Mater. **3**, 033604 (2019). Copyright 2019 American Physical Society. (b) Schematic illustration of an MPNN. (c) Representative RDC for an arbitrary system for neither different values of α, depicting the increasing resolution of the RDC with increasing α. Reprinted with permission from Madkhali *et al.*, Molecules **25**, 2715 (2020). Licensed under a Creative Commons Attribution (CC BY) license. (d) Time evolution of the *operando* Cr K-edge XANES spectra of a Cr<sup>VI</sup>/SiO<sub>2</sub> catalyst during reduction with ethylene (from black to red) and during ethylene polymerization (from red to bold orange). Reprinted with permission from Guda *et al.*, Catal. Today **336**, 3–21 (2019). Copyright 2019 Elsevier. (159)

K-edge XANES spectrum. 155 In particular, the authors examined two different representations of chemical space—the Coulomb matrix and the radial distribution curve (RDC) shown in Fig. 8(c)—to represent the local environment around an Fe absorption site and evaluated them based on their ability to recover the Fe K-edge XANES spectra of 9040 unique Fe-containing compounds. They concluded that RDC featurization can achieve smaller mean squared error (MSE) between the predicted and target XANES spectra more quickly and with fewer data samples, reinforcing the need for effective data representations of materials-specific descriptors. Rankine et al. built upon this work by implementing a deep neural network to estimate Fe K-edge XANES spectra, relying only on geometric information about the Fe local environment as input. 156 Specifically, the authors represented the local environment around the Fe absorption site by computing a discrete RDC comprising all two-body pairs within a fixed cutoff radius. Despite the limited input information, they demonstrated that a properly trained network can be used to make rapid, quantitatively accurate predictions of XANES spectra while circumventing the time and resource demands of advanced theoretical calculations.

Finally, one major advantage of XAS is its compatibility with diverse samples, both crystalline and amorphous, and sample environments, as in the case of in situ or operando measurements under extreme temperatures or externally applied fields, leading to diverse applications and opportunities for machine learning-assisted analysis. In particular, XAS is a prominent method used to correlate the structure of nanoparticle catalysts to properties such as catalytic activity, which is often characterized under the operando conditions of a harsh reaction environment, as shown in Fig. 8(d). Thus, the predictive ability of machine learning methods is attractive for directly recognizing encoded structural descriptors, such as coordination number, from evolving XAS spectral features. For example, Timoshenko et al. demonstrated that neural networks can be used to predict the average coordination numbers of Pt nanoparticles directly from their XANES spectra, which can then be used to determine particle sizes, shapes, and other structural motifs needed to inform catalyst design.1 Several successful examples of machine learning-aided analysis for operando XAS spectra of catalyst structures have been reported in recent years. 158-161 Machine learning has also been applied to conduct high-throughput screening and obtain additional chemical insight into the atomic configurations of thin films monitored by in situ XAS during synthesis. 162 Overall, machine learning methods have shown incredible potential for improving and accelerating the analysis of this versatile characterization tool, and more widespread integration of machine learning solutions within routine XAS analysis workflows may be on the horizon.

#### **B. Photoemission spectroscopies**

Contrary to XAS, which is generally bulk sensitive, photoelectron or photoemission spectroscopy (PES) is a surface-sensitive, photon-in, electron-out technique performed with light sources ranging from hard x rays to the extreme ultraviolet (UV) energy regime, which provides direct access to a material's electronic structure. 163,164 The high sensitivity of x-ray photoelectron spectroscopy (XPS) to the chemical environment makes it an essential tool for quantifying a material's composition. In this regard, machine learning–based fitting may be used to disentangle complex overlapping spectra. Aarva et al. used fingerprint spectra calculated with bonding motifs obtained from an

unsupervised clustering algorithm to fit x-ray photoelectron spectra.  $^{165}$  In another work, Drera et~al. trained a CNN using simulated spectra to predict chemical composition directly from multicomponent x-ray photoelectron spectra from a survey spectral library.  $^{166}$  To achieve high-quality training, an easy set  $\{x_j^E,y_j^E\}$  containing  $\sim \! 100\,000$  computed XPS examples is generated using electron scattering theory in the transport approximation, which is shown to generalize well to a set of  $\sim \! 500$  well-characterized experimental examples in the hard set  $\{x_j^H,y_j^H\}$ . Their approach obviates the need to fit these complex spectra directly while showing robustness against the contaminant signal within the survey spectra.

Apart from chemical quantification, modern PES with momentum-resolved detectors is capable of mapping the entire electronic structure of materials through multidimensional detection of photoelectron energy and momentum distributions. 163,167 The resulting 4D intensity data in energy-momentum space exhibit the same data structure as vibrational spectra obtained through inelastic scattering measurements. While this analogy implies transferability of machine learning approaches developed for inelastic scattering, to be discussed in Sec. III C, the relationship between PES observables and microscopic quantities is significantly more complex due to the quantum nature of the electronic states and the multiple prefactors that effectively modulate the intensity values in a momentum-dependent manner. 168 The current understanding of the complex photoemission spectra is limited by the available computational tools. Therefore, machine learning is a potential avenue to understanding such data. Highlighting the dispersive features is of primary importance for comparison between experiments and theories. For this task, robust methods are needed to tolerate the noise level and intensity modulations in the data. 169 Peng et al. trained a super-resolution neural network based on simulated angle-resolved PES (ARPES) data, the easy set  $\{x_i^E, y_i^E\}$ , to enhance the dispersive features in the experimental data, the hard set  $\{x_i^H, y_i^H\}$ , without explicit models of the band dispersion. <sup>170</sup> By contrast, Xian et al. cast band fitting as an inference problem and used a probabilistic graphical model to recover the underlying dispersion. Remarkably, this approach does not require training but a reasonably good prior guess as a starting point. Its reasonable computational scaling allows the reconstruction of multiband dispersions within the entire Brillouin zone, as demonstrated in the 2D material tungsten diselenide (WSe<sub>2</sub>).

#### C. Inelastic scattering

One of the major triumphs of neutron and x-ray characterization techniques is inelastic scattering, which measures the elementary excitations of materials.  $^{172-175}$  There are generally two types of elementary excitations at the meV energy range, including (a) collective atomic vibrations, such as phonons in crystalline solids  $^{176-180}$  and Boson peaks in amorphous materials,  $^{181-185}$  and (b) magnetic excitations, which are essential to understand the nature of strongly correlated materials,  $^{186}$  such as frustrated magnetic systems  $^{187-189}$  and unconventional superconductors.  $^{190-192}$  However, unlike elastic scattering, where massive synthetic data can be generated from forward models to build the easy set  $\{x_j^E,y_j^E\}$ , inelastic scattering is challenging for machine learning due to the atomistic origin and quantum nature of the excitations, where forward models have high computational cost. Therefore, one major hurdle for machine learning in the context of inelastic scattering is data scarcity. Here, we introduce two examples of

using machine learning to overcome this hurdle to study elementary excitations of phonons and magnetic excitations, respectively.

For machine learning-assisted phonon studies, Chen et al. built a neural network model that directly predicts a material's phonon density of states (DOS) using only the atomic coordinates and masses of its constituent atoms as input. 193 Two key challenges were addressed in this work. First, there was a lack of a large training set; a reliable density-functional perturbation theory (DFPT) database contains a only small set of  $\sim 1500$  examples. <sup>194</sup> Second, the predicted outcome, the phonon DOS, was a continuous function instead of a single scalar quantity. To tackle these challenges, a graph-based neural network termed the Euclidean neural network was implemented. Euclidean neural networks are by construction equivariant to permutation, 3D rotations, translations, and inversion and thus, fully respect crystallographic symmetry [Fig. 9(a)]. This inherent symmetry eliminates the need for data augmentation and enables the networks to generalize well without significant data volume. Intuitively, the symmetry constraint imposed on the operations of the neural network restricts the search space of functions to those that are physically meaningful; therefore, data become more powerful, and fewer data are needed to achieve accurate results that generalize well. The predicted phonon DOS is shown in Fig. 9(b), with each of the four rows representing an error quartile. For lower error predictions [first three rows in

Fig. 9(b)], the shape of DOS can be finely resolved; for high-error predictions [fourth row in Fig. 9(b)], coarse features such as bandwidth and DOS gaps can still largely be predicted. With such a predictive model available, the computational cost for phonon DOS is significantly reduced, and the prediction in alloy systems becomes feasible.

As for magnetic systems, Samarakoon et al. implemented an autoencoder to assist the estimation of magnetic Hamiltonian parameters {J} in the spin ice Dr<sub>2</sub>Ti<sub>2</sub>O<sub>7</sub>, including magnetic exchange coupling between neighboring spins and magnetic dipolar interactions.<sup>71</sup> Although the work considers diffuse scattering, which measures the static magnetic structure factor  $S(\mathbf{Q})$ , the architecture is also well suited for inelastic scattering with dynamical structure factor  $S(\mathbf{Q}, \omega)$ , since the forward model that obtains  $S(\mathbf{Q})$  from a parameterized Hamiltonian  $H\{J\}$  can also be used to calculate  $S(\mathbf{Q}, \omega)$ . The workflow is shown in Fig. 10. A Monte Carlo-based forward model is used to compute the simulated structure factor  $S^{\text{sim}}(\mathbf{Q})$ . Instead of directly comparing  $S^{\text{sim}}(\mathbf{Q})$  to  $S^{\text{exp}}(\mathbf{Q})$ , which could suffer from experimental artifacts, an autoencoder is applied to compress the structure factor  $S(\mathbf{Q})$  into a lower-dimensional, latent representation L where  $S_L = \{S_1, S_2, ..., S_D\}$ , with  $D = 30 < \dim\{\mathbf{Q}\}$ . The optimization process of the parameters  $\{J\}$  is then performed in the latent space of the autoencoder by comparing  $S_L^{\text{exp}}$  and  $S_L^{\text{sim}}$ . This example demonstrates a generic principle of how machine learning can aid inelastic

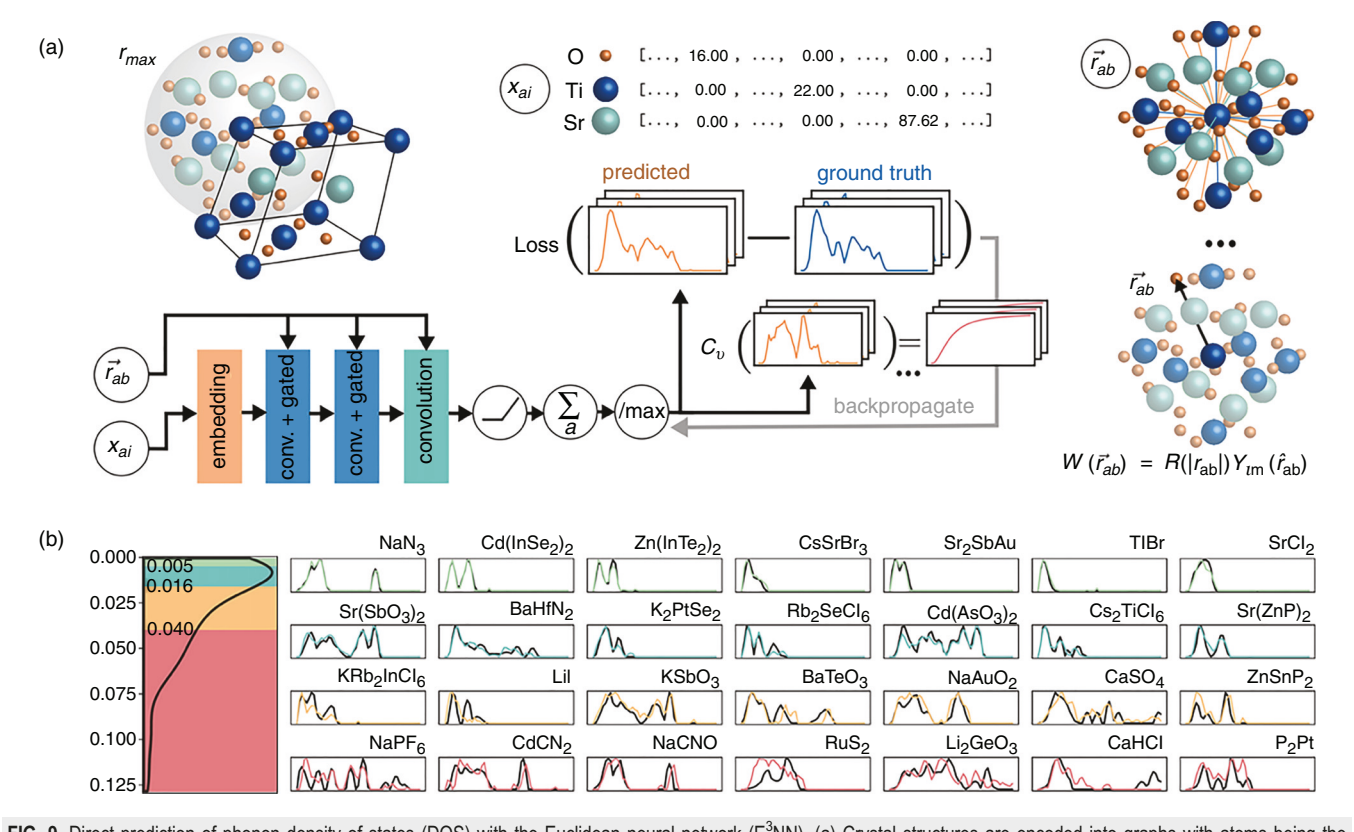
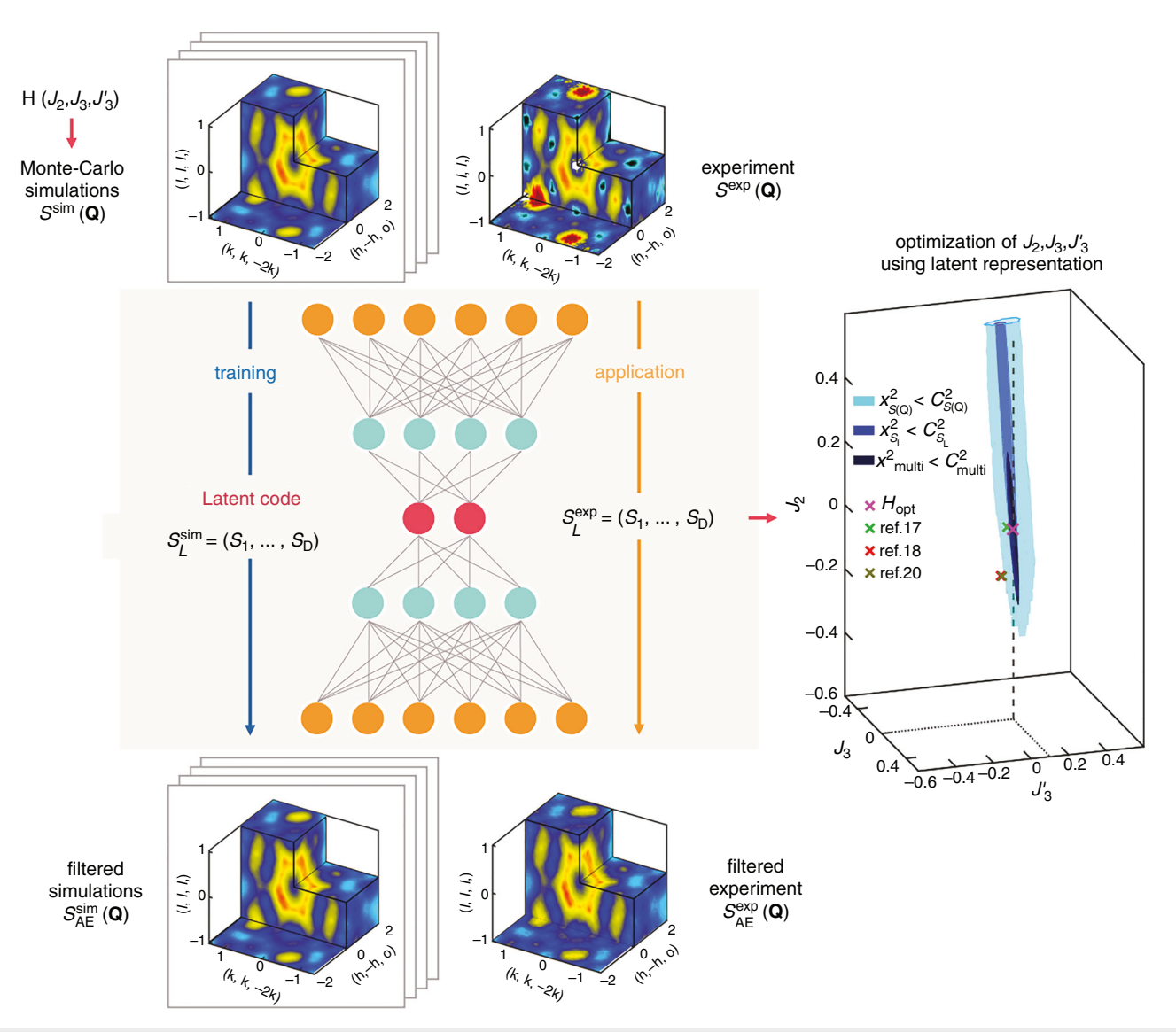


FIG. 9. Direct prediction of phonon density of states (DOS) with the Euclidean neural network (E<sup>3</sup>NN). (a) Crystal structures are encoded into graphs with atoms being the nodes with feature vectors and bonds being edges. The graph is then passed into the E<sup>3</sup>NN that preserves the crystallographic symmetry. (b) The predicted phonon DOS is displayed in four rows, with each representing an error quartile. Fine details of DOS can be well captured for samples in the first three rows (lower error predictions), while coarse features, such as bandwidth and DOS gap, can still be largely predicted for the last row (higher error predictions). Reprinted with permission from Chen et al., Adv. Sci. 2004214 (2021). Licensed under a Creative Commons Attribution (CC BY) license.



**FIG. 10.** Autoencoder-assisted Hamiltonian parameter estimation for experimentally measured magnetic structure factor  $S^{\text{exp}}(\mathbf{Q})$ . The autoencoder is trained with 1000 Monte Carlo-simulated data  $S^{\text{sim}}(\mathbf{Q})$  from the spin-ice Hamiltonian  $H(J_2,J_3,J_3')$ . To find a set of parameters  $\{J_2,J_3,J_3'\}$  that best represent experimental data, a cost function containing squared Euclidean distance in the learned latent space, namely  $\|S_L^{\text{exp}} - S_L^{\text{sim}}\|^2$ , is minimized. Reprinted with permission from Samarakoon *et al.*, Nat. Commun. 11, 892 (2020). Licensed under a Creative Commons Attribution (CC BY) license.

scattering to probe magnetic orderings and excitations. In particular, if the forward problem of calculating the dynamical structure factor  $S^{\text{sim}}(\mathbf{Q},\omega)$  from some parameterized Hamiltonian  $H\{J\}$  becomes feasible, for example using linear spin-wave theory, <sup>196</sup> we expect that similar machine learning models will have huge potential to study magnetic excitations with experimental data  $S^{\text{exp}}(\mathbf{Q},\omega)$  in strongly correlated systems.

# IV. EXPERIMENTAL INFRASTRUCTURE AND DATA A. Instrument and beam

Thus far, the discussion has focused on using machine learningaugmented elastic and inelastic scattering and spectroscopies to better elucidate materials properties. Given the central role of beamline infrastructure in a successful scattering experiment, machine learning has also been applied to optimize instrument operation,  $^{197-200}$  such as accurately characterizing x-ray pulse properties from a free-electron laser. Li *et al.* achieved dynamic aperture optimization using machine learning for the storage ring at the National Synchrotron Light II (NSLS-II) in Brookhaven National Laboratory (BNL). Dynamic aperture optimization aims to tune the configuration of the sextupole magnets to increase the ultra-relativistic electron lifetime in the storage ring. It is a multi-objective optimization problem with multiple objective functions  $f_m(\mathbf{x})$ ,  $m \geq 2$ , to minimize within the parameter space  $\{\mathbf{x}\}$ , which can be solved by a conventional multi-objective

genetic algorithm (MOGA) with further augmentation by machine learning. The direct tracking of a large number of particles forms a so-called "population" in the parameter space  $\{x\}$ ; Fig. 11(a) depicts example populations in a generic 2D parameter space  $(x_1,x_2)$ . Using k-means clustering, the populations are classified into different clusters, as shown in step 1 of Fig. 11(a). These clusters are further assigned a quality label [Fig. 11(a), step 2] by evaluating a fitness function, defined as the weighted average of objective functions  $F(\mathbf{x}) = \sum_{m=1}^{M} \omega_m f_m(\mathbf{x})$ , where the best or "elite" label corresponds to those populations that optimize the largest number of objective

functions  $f_m(\mathbf{x})$  (and have the longest electron lifetime in the storage ring). Finally, some proportion of candidates among the entire generation are replaced with potentially more competitive candidates repopulated within the range of the elite cluster [Fig. 11(a), step 3]. The replacement proportion in each intervention can further be dynamically adjusted or skipped based on a discrepancy score that compares the actual fitness value to that predicted by a k-nearest neighbor regression model. Here, the use of machine learning accelerates the convergence toward optimized parameters [Fig. 11(b)] and increases

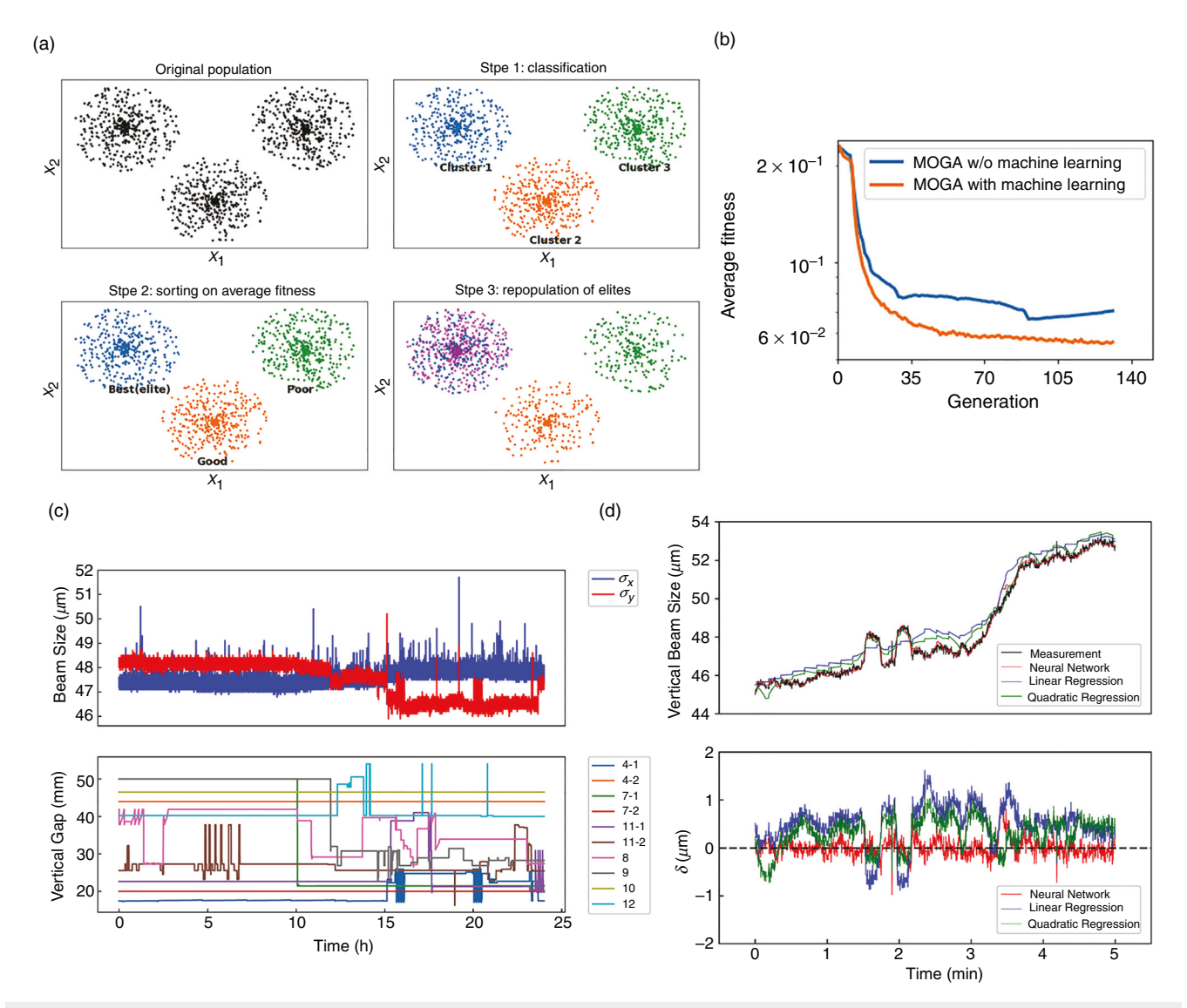


FIG. 11. Machine learning applications in scattering instruments and beams. (a) K-means clustering method is applied to classify parameter populations, where the regime of desired parameters is used to help to generate new candidates. (b) Faster convergence toward optimized parameters can be achieved with machine learning. Reprinted with permission from Li et al., Phys. Rev. Accel. Beams 21, 054601 (2018). Licensed under a Creative Commons Attribution (CC BY) license. (b) Variation in electron beam size (top) exists due to insertion device gaps (bottom). (d) A neural network is trained to accurately predict beam sizes based on insertion gaps; the comparisons on vertical beam sizes (top) and deviations of different model predictions (bottom) clearly show that the neural network can outperform regression models. Reprinted with permission from Leeman et al., Phys. Rev. Lett. 123, 194801 (2019). Copyright 2019 American Physical Society.

the number of high-quality elite candidates to reach longer-term electron beam stability in the storage ring.

In a different example, Leemann *et al.* applied machine learning to study the synchrotron source size stabilization from previous instrumental conditions at the Advanced Light Source (ALS) in Lawrence Berkeley National Laboratory (LBL).<sup>198</sup> The electron beam size can vary [Fig. 11(c), top] due to insertion device gaps [Fig. 11(c), bottom]. By constructing a neural network–based supervised learning model using the insertion device gaps or phase configurations as input and beam size as output, the authors achieved improved performance over simple regression models in accurately predicting the resulting beam sizes [Fig. 11(d)]. It is worth mentioning that the chosen fully connected artificial neural network contains three hidden layers and more parameters, which may approximate functions more complex than polynomial models and thus contribute the superior performance over polynomial regression models.

#### B. Data collection and processing

Machine learning can also facilitate the collection and processing of scattering data. Here, by "processing" we mean procedures like data refinement, denoising, automatic information–background segmentation, etc., but do not include the extraction of further materials information. Given how precious beamline resources are, the goal of machine learning in this context is to extract essential information with reduced beamtime. For diffractometry, one typical problem is diffraction peak–background segmentation, which usually requires that diffraction spots are collected with fine resolution. Sullivan *et al.* applied a deep U-Net to extract the shape of the Bragg peaks from time-of-flight neutron diffraction<sup>87</sup> and x-ray diffraction, which enables more reliable peak area integration. Training data are augmented by applying the following additional operations [Fig. 12(a)]:

 $x^E$  =histogramming, rotation, recentering, noise, cropping in reciprocal space

In another example, Ke *et al.* applied a CNN to identify diffraction spots from noisy data taken with an x-ray free-electron laser. <sup>88</sup>

For small-angle scattering, given the rapid drop of intensity at high Q (for a 3D object,  $I(Q) \propto Q^{-4}$ ) and limited beamtime resources, a typical problem is optimization of the data collection strategy in the high-Q regime. Asahara  $et\ al.$  applied Gaussian mixture modeling to predict longer-time SANS spectra by employing a prior from B-spline regression. The proposed B-spline Gaussian mixture model (BSGMM) outperforms conventional kernel density estimation (KDE) algorithms  $^{202}$  [Fig. 12(b)] and shortens the SANS experiment by a factor of five

Measurements can also be accelerated by reducing the number of necessary sampling points in a given parameter space with guidance from machine learning. Kanazawa *et al.* proposed a workflow that optimizes automatic sequential Q-sampling, which suggests the next Q-point based on uncertainties estimated from previously measured data<sup>203</sup> [Fig. 12(c)]. Noack and colleagues<sup>204,205</sup> have used kriging,<sup>206,207</sup> a Gaussian process regression method, to design an experimental sampling strategy in a spatially resolved SAXS measurement of block copolymer thin films. While a complete set of SAXS measurements is traditionally sampled using a regular grid, the authors showed that the use of kriging and its variants requires only a fraction of the

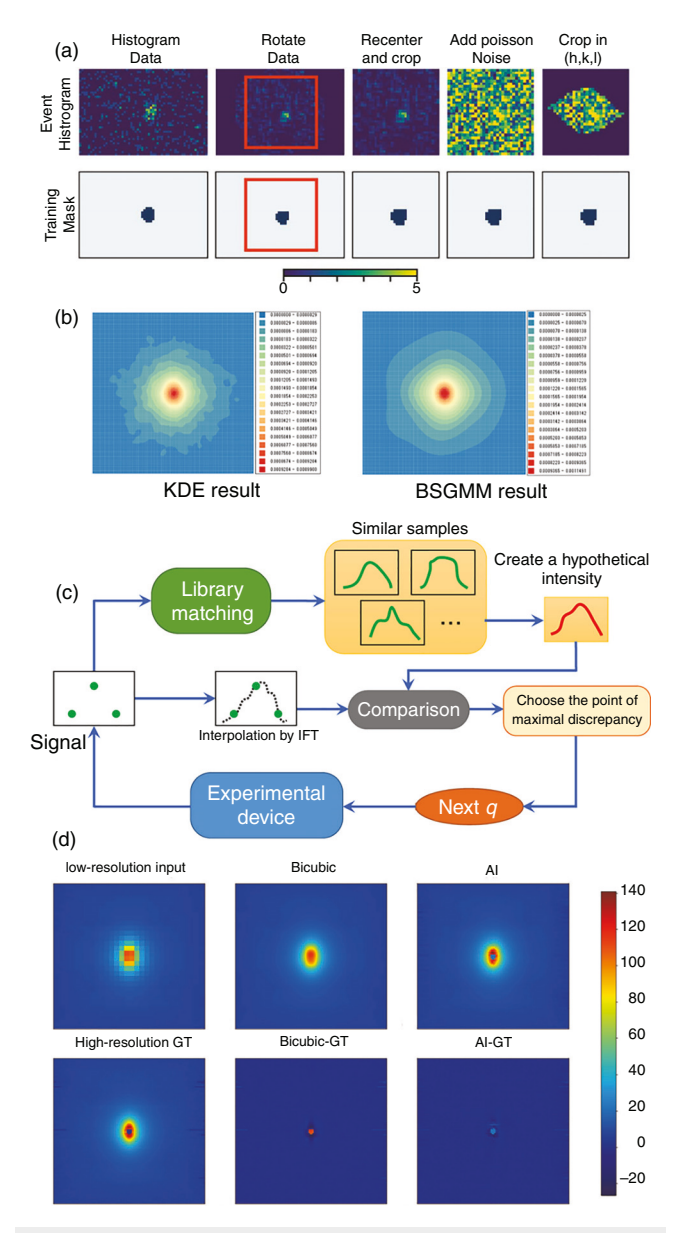


FIG. 12. Machine learning applications in collecting and processing scattering data. (a) Deep U-Net is applied to provide better peak masks for more accurate Bragg peaks integral. Reprinted with permission from Sullivan et al., J. Appl. Crystallogr. 52, 854-863 (2019). Copyright 2019 International Union of Crystallography. Predicted SANS pattern from traditional kernel density estimation (KDE) and B-spline Gaussian mixed model (BSGMM), where the latter approach yields smoother, suggesting better predictions are obtained. Reprinted with permission from Asahara et al., Proc. AAAI Conf. Artif. Intell. 33, 9410-9415 (2019). Copyright 2019 Association for the Advancement of Artificial Intelligence. 202 (c) Data-driven sequential measurement for SANS by proposing next sampling Q-points based on previously measured data. Reprinted with permission from Kanazawa et al., J. Phys. Mater. 3, 015001 (2019). Licensed under a Creative Commons Attribution (CC BY) license. (d) Comparisons of super-resolution for SANS data made by a CNN-based method and baseline bicubic upsampling algorithm, where the CNN-based method yields better reconstruction of the high-resolution data. Reprinted with permission from Chang et al., MRS Commun. 10, 11-17 (2020). Copyright 2020 Materials Research Society. 113 Al, artificial intelligence; IFT, inverse Fourier transform; GT, ground truth.

sampled spatial coordinates to arrive at a reconstruction with comparable detail to that produced by the grid scan. Their closed-loop approach highlights the potential for experimental automation to improve the efficiency in data acquisition and to maximize the information gathered from fragile samples.

Chang *et al.* addressed a similar challenge by applying a CNN to SANS spectral data to reach super-resolution. <sup>113</sup> Even for anisotropic scattering, the CNN-based super-resolution reconstruction has better agreement with the ground truth than the conventional bicubic algorithm [Fig. 12(d)].

Finally, machine learning can also be applied in problems that improve other data collection processes, such as calibrating the rotation axis for x-ray tomography, which improving the phase-contrast-spatial resolution contradiction in phase-contrast imaging, optimizing data segmentation in transmission x-ray microscopy (TXM), which is observed in the phase-contrast imaging, and achieving super-resolution in x-ray tomography.

#### V. OUTLOOK

#### A. Machine learning on time-resolved spectroscopies

A wide variety of machine learning models are available to study the dynamics of physical systems, for example, recurrent neural networks (RNNs) and RNN-based architectures. These architectures can be used for metamodeling of structural dynamics,<sup>213</sup> inferring quantum evolution of superconducting qubits,<sup>214</sup> and modeling quantum many-body systems on large lattices.<sup>215</sup> RNN-based models have also been applied to study nonlinear tomographic absorption spectra<sup>216</sup> and optical spectra from optoelectronic polymers.<sup>217</sup> However, the application of RNNs to time-resolved neutron or x-ray scattering experiments is still scarce. In the context of scattering measurements, additional challenges exist given that physical processes are represented by neutron or photon counts on detector arrays and experience noise and loss of phase information. Fortunately, neural networks are effective at denoising,<sup>218</sup> solving phase retrieval problems,<sup>219,220</sup> and handling missing information in time series data.<sup>221</sup> Thus, RNN-based models can serve as promising techniques to extract deeper insight from time-resolved neutron and x-ray spectra.

Neural ordinary differential equations (ODEs) are an alternative framework that can be used to learn from time series data. <sup>222</sup> As this framework can be intimately related to physical models, it is able to extrapolate well even with limited training data and has already found applications in modeling quantum phenomena. <sup>223,224</sup> As a result, it is interesting to consider how such physics-informed neural networks can perform in the context of neutron and x-ray scattering problems. Another approach for learning complex nonlinear dynamics is through deep Koopman operators. <sup>225,226</sup> In this technique, an autoencoder-like structure is developed to connect observed states with intrinsic states, represented by learned Koopman coordinates, which evolve within the latent space according to the learned system dynamics. Such an architecture can be analogously mapped to physical observables, such as scattering data, and the intrinsic quantum states of the measured samples and can thus serve as another promising approach to interpret time-resolved scattering data.

#### B. Leveraging information in real and reciprocal spaces

Frameworks that employ the principles of symmetry and Fourier transforms could efficiently learn models of complex physical systems and effectively represent scattering data in either real space, reciprocal space, or both. Symmetry and Fourier transforms are two of the most valuable and commonly used computational tools for tackling complex physics problems. These tools encode much of the domain knowledge we have about arbitrary scientific data in 3D space. First, the properties of physical systems (geometry and geometric tensor fields) transform predictably under rotations, translations, and inversions (3D Euclidean symmetry). Second, while physical systems can be described with equal accuracy in both real (position) space and reciprocal (momentum) space, some patterns and operations (e.g., convolutions, derivatives) are much simpler to identify or evaluate in one space than another. The beauty of symmetry and Fourier transforms is that they make no assumptions about the incoming data (only that they exist in 3D Euclidean space); this generality is also an opportunity for improvement. The strength of machine learning is the ability to build efficient algorithms by leveraging the context contained in a given dataset to forgo expensive computation.

A constant theme in scattering experiments is the acquisition of data in reciprocal space to inform something traditionally represented in real space. While there are models that can operate on these domains separately, it would be a valuable and natural direction to extend these methods to simultaneously operate and exchange information in both spaces. This exchange would also allow the user to input and output data in whichever space is more convenient and intuitive, and can directly support methods like diffraction imaging, which contain information in both spaces.

Using learnable context in combination with the fundamental principles of symmetry and Fourier transforms could help to alleviate some of the primary challenges associated with scattering experiments: missing phase information and sampling. Additionally, frameworks that can simultaneously compute in and exchange information between real and reciprocal space could naturally predict quasiparticle band structures from real space coordinates and express charge densities in terms of commonly used plane wave basis sets.

#### C. Multimodal machine learning

Materials characterization often requires insight from multiple experimental techniques with sensitivity to different types of excitations in order to gain a complete understanding of a material's properties and behaviors. Data acquired using different neutron and x-ray scattering techniques are often complementary but are typically synthesized manually by researchers. In this regard, machine learning may provide an important avenue toward intelligent analysis across multiple modalities. Multimodal machine learning<sup>227–230</sup> has already been explored for a range of versatile applications, including activity and context detection;<sup>231,232</sup> recognition of objects,<sup>233</sup> images,<sup>23</sup> emotions;<sup>235</sup> and improvement of certain medical diagnostics.<sup>23</sup> By consolidating information from multiple, complementary sources, multimodal machine learning models have the potential to make more robust predictions and discover more sophisticated relationships among data. At the same time, this approach introduces new prerequisites compared to learning from single modalities. The taxonomy by Baltrušaitis et al. considers five principal challenges of multimodal machine learning:<sup>229</sup> (1) representation of heterogeneous data; (2) translation, or mapping, of data from one modality to another; (3) alignment between elements of two or more different modalities; (4) fusion of information to perform a prediction; and (5) co-learning,

which considers how knowledge gained by learning from one modality can assist a model trained on a different modality whose resources may be more limited. These are likewise important considerations for the application of multimodal machine learning in the context of neutron and x-ray data analysis: Different experimental techniques access widely different energy, time, length, and momentum scales; produce diverse data structures; and carry varying levels of uncertainty. Additionally, developing the data infrastructure to aggregate measurements from multiple instruments would be an important undertaking for neutron and x-ray facilities as a whole. Nonetheless, intelligent synthesis of multiple experimental signatures appears to be a promising direction to better extract insights from data and possibly accelerate materials design and discovery.

## D. High-performance computing for quantum materials

Increasingly, studies in functional materials underscore emergent quantum phenomena that arise from entanglement. These quantum phenomena, such as quantum spin liquids, unconventional superconductivity, and many-body localization, are beyond the scope of an exclusively structural description and thus pose a challenge for reliable acquisition of high-quality training data for machine learning. Even so, the associated correlations in these materials are encoded in their inelastic scattering signatures, which motivates corresponding theoretical descriptions. Due to quantum entanglement, semiclassical theories like mean-field theory, linear spin-wave theory, or even DFT become insufficient because of their lack of static or dynamic electron correlations. Thus, machine learning and cross validation of spectroscopies associated with these materials require sophisticated computational methods. In addition to providing a high-throughput dataset for machine learning, recent studies have demonstrated that machine learning can benefit these numerical calculations by improving their efficiency and accuracy. 238,23

To sufficiently include quantum entanglement in spectral calculations, two promising routes have been attempted. The first route is the correction of DFT by embedding other methods. Beyond the elementary DFT + U corrections for total energy, the GW method allows a self-consistent correction of the Green's function using a screened Coulomb interaction in the random-phase approximation (RPA).<sup>24</sup> A more sophisticated correction for strong correlation effects is the DFT + DMFT (dynamical mean-field theory) method.<sup>241</sup> By mapping the self-energy into a single-site impurity problem, DMFT incorporates local high-order correlations into spectral calculations.<sup>242</sup> These corrections to DFT enable spectral calculations for materials with substantial quantum entanglement. However, as the corrections are usually biased, the accuracy of the results is sometimes not well controlled. The DFT + DMFT method has been widely used to simulate the single-particle Green's function relevant for photoemission experiments. 243 Its numerical complexity increases dramatically when extended to two-particle or four-particle correlation functions, which are required to evaluate inelastic scattering cross sections. Implemented using the Bethe-Salpeter equation and Lanczos method, the DFT + DMFT methods have been recently applied to the simulation of neutron scattering and resonant inelastic x-ray scattering (RIXS) spectra, <sup>244,245</sup> correctly reflecting the multiplet effects and Mott transition in transition metal materials. In light of these developments, it is, in principle, possible for hidden correlation information to be

revealed from spectra with proper training and selection of machine learning architectures.

The second route to include quantum entanglement is the construction of effective low-energy models based on ab initio Wannier orbitals and the evaluation of spectral properties based on these highly entangled effective models. Along this route, wavefunction-based methods, including exact diagonalization,<sup>246</sup> coupled clusters,<sup>247</sup> and density-matrix renormalization group (DMRG)<sup>248</sup> provide exact or asymptotically exact solutions to excited-state spectra for arbitrary strong correlations. The disadvantage of these wave function-based methods is that the rapid scaling of computational complexity restricts the calculations to only small systems or low dimensions with a limited number of bands. Another class of the model-based unbiased methods is quantum Monte Carlo, <sup>249</sup> which is less sensitive to the system's size but restricted by high temperature. These methods have been widely used in scattering spectrum calculations for spin liquids<sup>250</sup> and unconventional superconductors, <sup>251</sup> where spin correlations are dominant in a few bands. With constantly increasing computational power, we expect these techniques to play a more prominent role in future applications of machine learning to quantum materials.

Spectral calculations based on either route are computationally expensive and require massively parallel computing techniques. Most methods exhibit good scaling performance in distributed computing. With the reconstruction of bottom-level linear algebraic operations, these approaches have been further accelerated using the general-purpose graphics processing unit (GPGPU).

### E. Conclusion: Fundamental impact on experimental facilities

Beamtime at neutron and x-ray facilities is a limited and expensive scientific resource. This review outlines the remarkable impact that machine learning has had on scattering science in a very short span of time. The work so far shows a tantalizing glimpse of the way that these new approaches can revolutionize the collection, analysis, and interpretation of data and, in turn, the use and access to beamline facilities. Perhaps the most fundamental step under way is the use of machine learning to solve the inverse scattering problem [Fig. 2(a)]. The inversion of data to a model or representation is the goal of most experiments, whether it is to create a structural solution or to understand the couplings and dynamics in materials. It is a highly timeconsuming process that currently demands a great deal of expertise and, as such, is a major bottleneck in extracting meaningful scientific information. Training machine learning models using large-scale simulations provides an approach that finally addresses this bottleneck in a realistic way. A closely related problem is the treatment of experimental backgrounds and artifacts, which can also be addressed by artificial intelligence. Bringing these developments from machine learning into the realm of experiments through workflows and supporting computation is sure to have a fundamental impact throughout the neutron and x-ray scattering community.

There are a series of scattering and spectroscopy problems where artificial intelligence can be expected to make a significant impact in the foreseeable future. Machine learning approaches to SAS (Sec. II B) and XAS (Sec. III A) are well under way, and it can be expected that they will be implemented on beamlines in the near term to aid further automation of experiments and analysis. The problems of diffraction (Sec. II A), both on single crystal and powder samples, are at an earlier

stage. Here, the crucial problem is to improve the automation of finding structure solutions. Hybridizing these methods with more powerful optimization routines that can search for solutions in the very rugged landscape of the parameter space are likely to produce automated approaches, which would be transformative in the delivery of rapid materials understanding. Another aspect of diffraction experiments where the prospects of machine learning are especially promising is in the domain of diffuse scattering. A great deal of critical information about disorder and defects in materials is contained within the scattering between Bragg peaks. It has long been recognized that accessing this information would be very important, and the use of machine learning is proving to be well suited to this problem, especially in the case of magnetic materials. Large-scale simulations will open up this area for other applications, too. Finally, inelastic scattering data are particularly hard to visualize due to their fourdimensional nature. Experimentalists have trouble identifying not only underlying models but also what real features are present in the data (Sec. III C). Use of computationally efficient theoretical methods and simulations of instrumental effects can address this challenge and would change both the impact and the time frame of analyses. Finally, many experiments currently depend on high-purity single crystals, which are difficult and laborious to grow. Machine learning is showing that it is feasible to extract models from experimental data on powders instead of single crystals, which would promise much faster experimental throughput and turnaround in the understanding of materials.

The widespread deployment of machine learning can be expected to have a major impact on redefining the relationship between experimentation and modeling. Large-scale simulations used for training can also be used to explore phase diagrams of materials and identify underlying physical mechanisms. They also provide a powerful basis on which to steer experiments. Mining simulations present an opportunity to transform data interpretation, potentially giving enhanced significance to the results. Furthermore, experiments are conducted in high-dimensional parameter spaces of sample conditions, orientations, instrumental configurations, and counting times. Autonomous steering of experiments thus promises significant enhancement to experimental practice. Closing the loop between modeling and experimental control not only enables experiments that are otherwise too fast for humans to steer effectively but also allows the collection of information in scenarios that are too complex for conventional decision making.

Artificial intelligence is driving a change in the scale and speed of modeling as machine learning removes computational bottlenecks and provides the means to synthesize and compress simulations and their physical information content. This revolution will allow training and simulation over much wider classes of problems, potentially extending the scope of experiments. Integrating these advances in computational methods together with the needs of experiments is a key step that requires the fields of theory, applied mathematics, and computer science to work more closely with experimental science than ever before. To achieve these promising advances, federated data, curation, autonomous steering, and validated codes as well as new types of experimental groups, remote access, and team formation will need to be part of the future research landscape. The early indications of this change are very promising, and now is the time for researchers to explore machine learning as a powerful new capability that can transform neutron

and x-ray scattering, one of the most demanding and dataintensive branches of experimental science.

#### **ACKNOWLEDGMENTS**

Z.C., N.A., and M.L. acknowledge support from United States Department of Energy Basic Energy Sciences Award No. DE-SC0020148. N.A. acknowledges National Science Foundation (NSF) Graduate Research Fellowships Program support under Grant No. 1122374. Y.W. acknowledges support from NSF award DMR-2038011. R.P.X. and R.E. acknowledge the support by BiGmax, the Max Planck Society's Research Network on Big-Data-Driven Materials Science, and the European Research Council (ERC) under the European Union's Horizon 2020 Research and Innovation Program Grant No. ERC-2015-CoG-982843. DAT was supported by DOE BES User Facilities.

#### **DATA AVAILABILITY**

Data sharing is not applicable to this article as no new data were created or analyzed in this study.

#### **REFERENCES**

- <sup>1</sup>S. W. Lovesey, *Theory of Neutron Scattering from Condensed Matter* (Clarendon Press, 1984).
- <sup>2</sup>J. Als-Nielsen and D. McMorrow, *Elements of Modern X-Ray Physics*, 2nd ed (Wiley, 2011).
- <sup>3</sup>F. Bohn et al., "European Source of Science," ESS Project 1 (2002).
- <sup>4</sup>U.S. National Research Council, Committee on Atomic Molecular and Optical Sciences 2010, Controlling the Quantum World: The Science of Atoms, Molecules, and Photons (National Academies Press, 2007).
- <sup>5</sup>M. Yabashi and H. Tanaka, "The next ten years of X-ray science," Nat. Photonics 11, 12–14 (2017).
- <sup>6</sup>X. D. Su *et al.*, "Protein crystallography from the perspective of technology developments," Crystallogr. Rev. **21**, 122–153 (2015).
- O. G. Shpyrko, "X-ray photon correlation spectroscopy," J. Synchrotron. Radiat. 21, 1057–1064 (2014).
- <sup>8</sup>K. P. Murphy, *Machine Learning: A Probabilistic Perspective* (MIT Press, 2012).
- <sup>9</sup>I. Goodfellow, Y. Bengio, and A. Courville, *Deep Learning* (The MIT Press, 2016).
- <sup>10</sup>S. L. Brunton, J. L. Proctor, and J. N. Kutz, "Discovering governing equations from data by sparse identification of nonlinear dynamical systems," Proc. Nat. Acad. Sci. 113, 3932 (2016).
- <sup>11</sup>K. Kaheman, E. Kaiser, B. Strom, J. N. Kutz, and S. L. Brunton, "Learning discrepancy models from experimental data," arXiv:1909.08574 (2019).
- <sup>12</sup>C. Rackauckas et al., "Universal differential equations for scientific machine learning," arXiv:2001.04385 (2020).
- <sup>13</sup>M. Y. Niu, L. Horesh, and I. Chuang, "Recurrent neural networks in the eye of differential equations," arXiv:1904.12933 (2019).
- <sup>14</sup>A. Sherstinsky, "Fundamentals of recurrent neural network (RNN) and long short-term memory (LSTM) network," Phys. D Nonlinear Phenom. 404, 133306 (2020)
- <sup>15</sup>B. M. De Silva, D. M. Higdon, S. L. Brunton, and J. N. Kutz, "Discovery of physics from data: Universal laws and discrepancies," Front. Artif. Intell. 3, 00025 (2020).
- <sup>16</sup>K. T. Schütt *et al.*, "How to represent crystal structures for machine learning: Towards fast prediction of electronic properties," Phys. Rev. B **89**, 205118 (2014).
- <sup>17</sup>K. T. Schütt *et al.*, "SchNet: A continuous-filter convolutional neural network for modeling quantum interactions," arXiv:1706.08566 (2017).
- <sup>18</sup> K. T. Schütt, H. E. Sauceda, P.-J. Kindermans, A. Tkatchenko, and K.-R. Müller, "SchNet A deep learning architecture for molecules and materials," J. Chem. Phys. 148, 241722 (2018).
- <sup>19</sup>N. Thomas, T. Smidt, S. Kearnes, L. Yang, L. Li, K. Kohlhoff, and P. Riley, "Tensor field networks: Rotation- and translation-equivariant neural networks for 3D point clouds," arXiv:1802.08219 (2018).

- <sup>20</sup>B. K. Miller, M. Geiger, T. E. Smidt, and F. Noé, "Relevance of rotationally equivariant convolutions for predicting molecular arXiv:2008.08461 (2020).
- <sup>21</sup>K. T. Schütt, F. Arbabzadah, S. Chmiela, K. R. Müller, and A. Tkatchenko, "Quantum-chemical insights from deep tensor neural networks," Nat. Commun. 8, 13890 (2017).
- <sup>22</sup>K. T. Schütt, M. Gastegger, A. Tkatchenko, K. R. Müller, and R. J. Maurer, "Unifying machine learning and quantum chemistry with a deep neural network for molecular wavefunctions," Nat. Commun. 10, 5024 (2019).
- <sup>23</sup>G. P. P. Pun, R. Batra, R. Ramprasad, and Y. Mishin, "Physically informed artificial neural networks for atomistic modeling of materials," Nat. Commun.10, 2339 (2019).
- 24T. Xie and J. C. Grossman, "Crystal graph convolutional neural networks for an accurate and interpretable prediction of material properties," Phys Rev. Lett. 120, 145301 (2018).
- 25 T. Xie, A. France-Lanord, Y. Wang, Y. Shao-Horn, and J. C. Grossman, "Graph dynamical networks for unsupervised learning of atomic scale dynamics in materials," Nat. Commun. 10, 2667 (2019).
- <sup>26</sup>C. Chen, W. Ye, Y. Zuo, C. Zheng, and S. P. Ong, "Graph networks as a universal machine learning framework for molecules and crystals," Chem. Mater. 31, 3564-3572 (2019).
- <sup>27</sup>T. Hey, K. Butler, S. Jackson, and J. Thiyagalingam, "Machine learning and big scientific data," Philos. Trans. A Math. Phys. Eng. Sci. 378, 20190054
- <sup>28</sup>O. Isayev et al., "Universal fragment descriptors for predicting properties of inorganic crystals," Nat. Commun. 8, 15679 (2017).
- <sup>29</sup>G. Pilania, C. Wang, X. Jiang, S. Rajasekaran, and R. Ramprasad, "Accelerating materials property predictions using machine learning," Sci. Rep. 3, 2810 (2013).
- 30 J. Carrete, W. Li, N. Mingo, S. Wang, and S. Curtarolo, "Finding unprecedentedly low-thermal-conductivity half-Heusler semiconductors via highthroughput materials modeling," Phys. Rev. X 4, 011019 (2014).
- <sup>31</sup>S. A. Tawfik, O. Isayev, M. J. S. Spencer, and D. A. Winkler, "Predicting thermal properties of crystals using machine learning," Adv. Theory Simul. 3, 201900208 (2019).
- 32 A. van Roekeghem, J. Carrete, C. Oses, S. Curtarolo, and N. Mingo, "Highthroughput computation of thermal conductivity of high-temperature solid phases: The case of oxide and fluoride perovskites," Phys. Rev. X 6, 041061
- 33Y. Dong et al., "Bandgap prediction by deep learning in configurationally hybridized graphene and boron nitride," npj Comput. Mater. 5, 26 (2019).
- <sup>34</sup>B. Meredig *et al.*, "Can machine learning identify the next high-temperature superconductor? Examining extrapolation performance for materials discovery," Mol. Syst. Des. Eng. 3, 819-825 (2018).
- 35 M. S. Scheurer and R. J. Slager, "Unsupervised machine learning and band topology," Phys. Rev. Lett. 124, 226401 (2020).
- <sup>36</sup>V. Stanev *et al.*, "Machine learning modeling of superconducting critical temperature," npj Comput. Mater. 4, 29 (2018).
- <sup>37</sup>L. Ward, A. Agrawal, A. Choudhary, and C. Wolverton, "A general-purpose machine learning framework for predicting properties of inorganic materials," npj Comput. Mater. 2, 16028 (2016).
- <sup>38</sup>Y. Zhuo, A. Mansouri Tehrani, and J. Brgoch, "Predicting the band gaps of inorganic solids by machine learning," J. Phys. Chem. Lett. 9, 1668-1673 (2018).
- <sup>39</sup>N. Andrejevic, J. Andrejevic, C. H. Rycroft, and M. Li, "Machine learning spectral indicators of topology," arXiv:2003.00994 (2020).
- <sup>40</sup>R. Gomez-Bombarelli *et al.*, "Automatic chemical design using a data-driven continuous representation of molecules," ACS Cent. Sci. 4, 268-276 (2018).
- 41Y. Liu, T. Zhao, W. Ju, and S. Shi, "Materials discovery and design using machine learning," J. Materiomics 3, 159–177 (2017).

  <sup>42</sup>A. O. Oliynyk *et al.*, "High-throughput machine-learning-driven synthesis of
- full-Heusler compounds," Chem. Mater. 28, 7324-7331 (2016).
- <sup>43</sup>P. Raccuglia *et al.*, "Machine-learning-assisted materials discovery using failed experiments," Nature 533, 73–76 (2016).

  44J. Noh *et al.*, "Inverse design of solid-state materials via a continuous repre-
- sentation," Matter 1, P1370-P1384 (2019).

- 45S. Kim, J. Noh, G. H. Gu, A. Aspuru-Guzik, and Y. Jung, "Generative adversarial networks for crystal structure prediction," ACS Cent. Sci. 6, 1412-1420
- <sup>46</sup>P. Ronhovde *et al.*, "Detecting hidden spatial and spatio-temporal structures in glasses and complex physical systems by multiresolution network clustering," Eur. Phys. J. E Soft. Matter 34, 105 (2011).
- <sup>47</sup>P. Ronhovde et al., "Detection of hidden structures for arbitrary scales in complex physical systems," Sci. Rep. 2, 329 (2012).
- 48Z. Nussinov et al., in Information Science for Materials Discovery and Design, edited by T. Lookman, F. J. Alexander, and K. Rajan (Springer International Publishing, 2016), pp. 115-138.
- 49 V. Botu, R. Batra, J. Chapman, and R. Ramprasad, "Machine learning force fields: Construction, validation, and outlook," J. Phys. Chem. C 121, 511-522 (2016)
- 50 A. Glielmo, P. Sollich, and A. De Vita, "Accurate interatomic force fields via machine learning with covariant kernels," Phys. Rev. B 95, 214302 (2017).
- <sup>51</sup>I. Kruglov, O. Sergeev, A. Yanilkin, and A. R. Oganov, "Energy-free machine learning force field for aluminum," Sci. Rep. 7, 8512 (2017).
- 52Z. Li, J. R. Kermode, and A. De Vita, "Molecular dynamics with on-the-fly machine learning of quantum-mechanical forces," Phys. Rev. Lett. 114, 096405 (2015).
- 53L. Zhang, D.-Y. Lin, H. Wang, R. Car, and W. E, "Active learning of uniformly accurate interatomic potentials for materials simulation," Phys. Rev. Mater. 3, 023804 (2019).
- 54B. Mortazavi et al., "Machine-learning interatomic potentials enable firstprinciples multiscale modeling of lattice thermal conductivity in graphene/ borophene heterostructures," Mater. Horiz. 7, 2359-2367 (2020).
- <sup>55</sup>V. L. Deringer *et al.*, "Origins of structural and electronic transitions in disordered silicon," Nature 589, 59-64 (2021).
- <sup>56</sup>K. T. Butler, D. W. Davies, H. Cartwright, O. Isayev, and A. Walsh, "Machine learning for molecular and materials science," Nature 559, 547-555 (2018).
- <sup>57</sup>M. Rupp, "Machine learning for quantum mechanics in a nutshell," Int. J. Quantum Chem. 115, 1058-1073 (2015).
- 58 J. Schmidt, M. R. G. Marques, S. Botti, and M. A. L. Marques, "Recent advances and applications of machine learning in solid-state materials science," npj Comput. Mater. 5, 83 (2019).
- <sup>59</sup>P. Mehta *et al.*, "A high-bias, low-variance introduction to machine learning for physicists," Phys. Rep. 810, 1-124 (2019).
- 60G. Carleo et al., "Machine learning and the physical sciences," Rev. Mod. Phys. 91, 045002 (2019).
- <sup>61</sup>R. Batra, L. Song, and R. Ramprasad, "Emerging materials intelligence ecosystems propelled by machine learning," Nat. Rev. Mater. (published online).
- <sup>62</sup>C. Suh, C. Fare, J. A. Warren, and E. O. Pyzer-Knapp, "Evolving the materials genome: How machine learning is fueling the next generation of materials discovery," Annu. Rev. Mater. Res. 50, 1-25 (2020).
- <sup>63</sup>D. H. Wolpert and W. G. Macready, "No free lunch theorems for optimization," IEEE Trans. Evol. Comput. 1, 67-82 (1997).
- <sup>64</sup>M. Rupp, A. Tkatchenko, K. R. Muller, and O. A. von Lilienfeld, "Fast and accurate modeling of molecular atomization energies with machine learning," Phys. Rev. Lett. 108, 058301 (2012).
- 65 F. Faber, A. Lindmaa, O. A. von Lilienfeld, and R. Armiento, "Crystal structure representations for machine learning models of formation energies," Int. J. Quantum Chem. 115, 1094-1101 (2015).
- 66J. Behler and M. Parrinello, "Generalized neural-network representation of high-dimensional potential-energy surfaces," Phys. Rev. Lett. 98, 146401
- 67 A. P. Bartók, R. Kondor, and G. Csányi, "On representing chemical environments," Phys. Rev. B 87, 184115 (2013).
- <sup>68</sup>J. Hoffmann *et al.*, "Data-driven approach to encoding and decoding 3-D crystal structures," arXiv:1909.00949 (2019).
- <sup>69</sup>O. Ronneberger, P. Fischer, and T. Brox, "U-Net: Convolutional networks for biomedical image segmentation," in International Conference on Medical Image Computing and Computer-Assisted Intervention (Springer, 2018), pp. 234-241.
- 70 D. P. Kingma and M. Welling, "Auto-encoding variational bayes," arXiv:1312.6114 (2013).

- <sup>71</sup>A. M. Samarakoon *et al.*, "Machine-learning-assisted insight into spin ice Dy2Ti2O7," Nat. Commun. 11, 892 (2020).
- 72I. J. Goodfellow et al., "Generative adversarial nets," in NIPS'14: Proceedings of the 27th International Conference on Neural Information Processing Systems (Association for Computing Machinery, 2014), Vol. 2, pp. 2672–2680
- <sup>73</sup>M. G. Maurice Weiler, M. Welling, W. Boomsma, and T. Cohen, "3D steerable CNNs: Learning rotationally equivariant features in volumetric data," in 32nd Conference on Neural Information Processing Systems 2018 (Neural Information Processing Systems Foundation, 2018), pp. 10381–10392.
- <sup>74</sup>Z. L. Risi Kondor and S. Trivedi, "Clebsch–Gordan nets: A fully Fourier space spherical convolutional neural network," in 32nd Conference on Neural Information Processing Systems 2018 (Neural Information Processing Systems Foundation, 2018).
- 75P. Paatero and U. Tapper, "Positive matrix factorization: A non-negative factor model with optimal utilization of error estimates of data values," Environmetrics 5, 111–126 (1994).
- <sup>76</sup>D. D. Lee and H. S. Seung, "Learning the parts of objects by non-negative matrix factorization," Nature 401, 788–791 (1999).
- <sup>77</sup>D. Kitamura et al., "Robust music signal separation based on supervised non-negative matrix factorization with prevention of basis sharing," in *IEEE International Symposium on Signal Processing and Information Technology* (IEEE, 2013), pp. 000392–000397.
- <sup>78</sup>G. Kim *et al.*, "First-principles and machine learning predictions of elasticity in severely lattice-distorted high-entropy alloys with experimental validation," Acta Materialia 181, 124–138 (2019).
- <sup>79</sup>C. Garcia-Cardona *et al.*, "Learning to predict material structure from neutron scattering data," IEEE Int. Conf. Big. Data 4490–4497 (2019).
- 80 F. Oviedo et al., "Fast and interpretable classification of small X-ray diffraction datasets using data augmentation and deep neural networks," npj Comput. Mater. 5, 60 (2019).
- <sup>81</sup>C. H. Liu, Y. Z. Tao, D. Hsu, Q. Du, and S. J. L. Billinge, "Using a machine learning approach to determine the space group of a structure from the atomic pair distribution function," Acta Crystallogr. A 75, 633–643 (2019).
- 82D. Olds et al., "Precise implications for real-space pair distribution function modeling of effects intrinsic to modern time-of-flight neutron diffractometers," Acta Crystallogr. A Found. Adv. 74, 293–307 (2018).
- 83 J. Bai et al., "Phase mapper: Accelerating materials discovery with AI," AI Mag. 39, 15–26 (2018).
- 84C. J. Long, D. Bunker, X. Li, V. L. Karen, and I. Takeuchi, "Rapid identification of structural phases in combinatorial thin-film libraries using x-ray diffraction and non-negative matrix factorization," Rev. Sci. Instrum. 80, 103902 (2009).
- 85 V. Stanev et al., "Unsupervised phase mapping of X-ray diffraction data by nonnegative matrix factorization integrated with custom clustering," npj Comput. Mater. 4, 43 (2018).
- 86J. Venderley et al., "Harnessing interpretable and unsupervised machine learning to address big data from modern x-ray diffraction," arXiv:2008.03275 (2020).
- 87B. Sullivan et al., "Volumetric segmentation via neural networks improves neutron crystallography data analysis," IEEE ACM Int. Symp. 549–555 (2019).
- <sup>88</sup>T. W. Ke *et al.*, "A convolutional neural network-based screening tool for X-ray serial crystallography," J. Synchrotron Radiat. **25**, 655–670 (2018).
- 89B. Sullivan et al., "BraggNet: Integrating Bragg peaks using neural networks," J. Appl. Crystallogr. 52, 854–863 (2019).
- <sup>90</sup>Y. T. Song, N. Tamura, C. B. Zhang, M. Karami, and X. Chen, "Data-driven approach for synchrotron x-ray Laue microdiffraction scan analysis," Acta Crystallogr. A 75, 876–888 (2019).
- <sup>91</sup>J. Rodman, Y. W. Lin, D. Sprouster, L. Ecker, and S. Yoo, "Automated X-ray diffraction of irradiated materials," in 2017 New York Scientific Data Summit (NYSDS) (IEEE, 2017), pp. 1–3.
- (NYSDS) (IEEE, 2017), pp. 1–3.

  92G. Viswanathan *et al.*, "Single-Crystal Automated Refinement (SCAR): A data-driven method for determining inorganic structures," Inorg. Chem. 58, 9004–9015 (2019).
- 93O. Glatter and O. Kratky, Small Angle x-Ray Scattering (Academic Press, 1982)

- <sup>94</sup>D. I. Svergun, L. A. Feigin, and G. W. Taylor, Structure Analysis by Small-Angle X-Ray and Neutron Scattering (Plenum Press, 1987).
- 95S. K. Sinha, E. B. Sirota, S. Garoff, and H. B. Stanley, "X-ray and neutron-scattering from rough surfaces," Phys. Rev. B 38, 2297–2311 (1988).
- 96J. S. Pedersen, "Analysis of small-angle scattering data from colloids and polymer solutions: Modeling and least-squares fitting," Adv. Colloid Interface Sci. 70, 171–210 (1997).
- <sup>97</sup>B. Chu and B. S. Hsiao, "Small-angle X-ray scattering of polymers," Chem. Rev. 101, 1727–1761 (2001).
- 98 R. J. Roe, Methods of X-Ray and Neutron Scattering in Polymer Science (Oxford University Press, 2000).
- <sup>99</sup>M. H. J. Koch, P. Vachette, and D. I. Svergun, "Small-angle scattering: A view on the properties, structures and structural changes of biological macromolecules in solution," Q. Rev. Biophys. 36, 147–227 (2003).
- 100 R. Ashkar et al., "Neutron scattering in the biological sciences: Progress and prospects," Acta Crystallogr. D Struct. Biol. 74, 1129–1168 (2018).
- 101E. E. Lattman, T. D. Grant, and E. H. Snell, Biological Small Angle Scattering: Theory and Practice, 1st ed (Oxford University Press, 2018).
- 102S. Mühlbauer et al., "Magnetic small-angle neutron scattering," Rev. Mod. Phys. 91, 015004 (2019).
- 103P. Das et al., "Small-angle neutron scattering study of vortices in superconducting Ba(Fe<sub>0.93</sub>Co<sub>0.07</sub>)<sub>2</sub>As<sub>2</sub>," Supercond. Sci. Technol. 23, 054007 (2010).
- 104 M. R. Eskildsen, E. M. Forgan, and H. Kawano-Furukawa, "Vortex structures, penetration depth and pairing in iron-based superconductors studied by small-angle neutron scattering," Rep. Prog. Phys. 74, 124504 (2011).
- 105 Y. Li, N. Egetenmeyer, J. L. Gavilano, N. Barišić, and M. Greven, "Magnetic vortex lattice in HgBa2CuO4+δ observed by small-angle neutron scattering," Phys. Rev. B 83, 054507 (2011).
- <sup>106</sup>E. Y. Lee, B. M. Fulan, G. C. L. Wong, and A. L. Ferguson, "Mapping membrane activity in undiscovered peptide sequence space using machine learning," Proc. Natl. Acad. Sci. U.S.A. 113, 13588–13593 (2016).
- 107B. Y. Wang, K. Yager, D. T. Yu, and M. Hoai, "X-ray scattering image classification using deep learning," IEEE Wint. Conf. Appl. 697–704 (2017).
- <sup>108</sup>D. Franke, C. M. Jeffries, and D. I. Svergun, "Machine learning methods for x-ray scattering data analysis from biomacromolecular solutions," Biophys. J. 114, 2485–2492 (2018).
- 109O. Demerdash et al., "Using small-angle scattering data and parametric machine learning to optimize force field parameters for intrinsically disordered proteins," Front. Mol. Biosci. 6, 64 (2019).
- <sup>110</sup>G. L. Hura *et al.*, "Small angle X-ray scattering-assisted protein structure prediction in CASP13 and emergence of solution structure differences," Proteins 87, 1298–1314 (2019).
- <sup>111</sup>S. Liu et al., "Convolutional neural networks for grazing incidence x-ray scattering patterns: Thin film structure identification," MRS Commun. 9, 586–592 (2019).
- <sup>112</sup>R. K. Archibald *et al.*, "Classifying and analyzing small-angle scattering data using weighted k nearest neighbors machine learning techniques," J. Appl. Crystallogr. 53, 326–334 (2020).
- <sup>113</sup>M.-C. Chang, Y. Wei, W.-R. Chen, and C. Do, "Deep learning-based super-resolution for small-angle neutron scattering data: Attempt to accelerate experimental workflow," MRS Commun. 10, 11–17 (2020).
- <sup>114</sup>Y. L. Chen and L. Pollack, "Machine learning deciphers structural features of RNA duplexes measured with solution X-ray scattering," IUCr J. 7, 870–880 (2020).
- <sup>115</sup>C. Do, W.-R. Chen, and S. Lee, "Small angle scattering data analysis assisted by machine learning methods," MRS Adv. 5, 1577–1584 (2020).
- <sup>116</sup>H. He, C. Liu, and H. Liu, "Model reconstruction from small-angle x-ray scattering data using deep learning methods," iScience 23, 100906 (2020).
- <sup>117</sup>H. Ikemoto et al., "Classification of grazing-incidence small-angle X-ray scattering patterns by convolutional neural network," J. Synchrotron Radiat. 27, 1069–1073 (2020).
- <sup>118</sup>A. Lyoussi *et al.*, "Deep learning methods on neutron scattering data," EPJ Web Conferences 225, 01004 (2020).
- <sup>119</sup>N. Kardjilov, I. Manke, A. Hilger, M. Strobl, and J. Banhart, "Neutron imaging in materials science," Mater. Today 14, 248–256 (2011).
- <sup>120</sup>N. Kardjilov, I. Manke, R. Woracek, A. Hilger, and J. Banhart, "Advances in neutron imaging materials," Mater. Today 21, 652–672 (2018).

- <sup>121</sup>C. J. Jacobsen, X-Ray Microscopy (Cambridge University Press, 2020).
- 122B. J. Erickson, P. Korfiatis, Z. Akkus, and T. L. Kline, "Machine learning for medical imaging," RadioGraphics 37, 505–515 (2017).
- 123G. Wang, J. C. Ye, and B. De Man, "Deep learning for tomographic image reconstruction," Nat. Mach. Intell. 2, 737–748 (2020).
- 124D. M. Pelt and K. J. Batenburg, "Fast tomographic reconstruction from limited data using artificial neural networks," IEEE Trans. Image Process. 22, 5238–5251 (2013).
- 125D. Micieli, T. Minniti, L. M. Evans, and G. Gorini, "Accelerating neutron tomography experiments through artificial neural network based reconstruction," Sci. Rep. 9, 2450 (2019).
- 126 X. Yang et al., "Tomographic reconstruction with a generative adversarial network," J. Synchrotron Radiat. 27, 486–493 (2020).
- 127X. G. Zhang, J. J. Xu, and G. Y. Ge, "Defects recognition on X-ray images for weld inspection using SVM," in *Proceedings of the 2004 International Conference on Machine Learning and Cybernetics* (IEEE, 2004), Vols. 1–7, pp. 3721–3725.
- 128A. P. Rale, D. C. Gharpure, and V. R. Ravindran, "Comparison of different ANN techniques for automatic defect detection in X-Ray Images," in 2009 International Conference on Emerging Trends in Electronic and Photonic Devices and Systems (ELECTRO-2009) (IEEE, 2009), p. 193.
- <sup>129</sup>A. Rovinelli, M. D. Sangid, H. Proudhon, and W. Ludwig, "Using machine learning and a data-driven approach to identify the small fatigue crack driving force in polycrystalline materials," npj Comput. Mater. 4, 35 (2018).
- <sup>130</sup>P. I. Guntoro, G. Tiu, Y. Ghorbani, C. Lund, and J. Rosenkranz, "Application of machine learning techniques in mineral phase segmentation for X-ray microcomputed tomography (μCT) data," Miner. Eng. 142, 105882 (2019).
- <sup>131</sup>D. Y. Parkinson et al., "Machine learning for micro-tomography," Proc. SPIE 10391, 103910J (2017).
- 132]. M. Earles et al., "In vivo quantification of plant starch reserves at micrometer resolution using X-ray microCT imaging and machine learning," New Phytol. 218, 1260–1269 (2018).
- 133 A. Z. Abidin et al., "Deep transfer learning for characterizing chondrocyte patterns in phase contrast X-Ray computed tomography images of the human patellar cartilage," Comput. Biol. Med. 95, 24–33 (2018).
- <sup>134</sup>M. Beliaev *et al.*, "Quantification of sheet nacre morphogenesis using x-ray nanotomography and deep learning," J. Struct. Biol. **209**, 107432 (2020).
- 135 J. Miao, P. Charalambous, J. Kirz, and D. Sayre, "Extending the methodology of x-ray crystallography to allow imaging of micrometre-sized non-crystalline specimens," Nature 400, 342–344 (1999).
- <sup>136</sup>J. Miao, T. Ishikawa, I. K. Robinson, and M. M. Murnane, "Beyond crystallog-raphy: Diffractive imaging using coherent x-ray light sources," Science 348, 530–535 (2015).
- 137 F. Pfeiffer, "X-ray ptychography," Nat. Photonics 12, 9–17 (2017).
- 138B. Langbehn et al., "Three-dimensional shapes of spinning helium nano-droplets," Phys. Rev. Lett. 121, 255301 (2018).
- 1359J. Zimmermann et al., "Deep neural networks for classifying complex features in diffraction images," Phys. Rev. E 99, 063309 (2019).
- 140 M. J. Cherukara et al., "Al-enabled high-resolution scanning coherent diffraction imaging," Appl. Phys. Lett. 117, 044103 (2019).
- <sup>141</sup>A. Scheinker and R. Pokharel, "Adaptive 3D convolutional neural network-based reconstruction method for 3D coherent diffraction imaging," J. Appl. Phys. 128, 184901 (2020).
- <sup>142</sup>M. Du, Y. S. G. Nashed, S. Kandel, D. Gürsoy, and C. Jacobsen, "Three dimensions, two microscopes, one code: Automatic differentiation for x-ray nanotomography beyond the depth of focus limit," Sci. Adv. 6, eaay3700 (2020).
- 143G. Ongie et al., "Deep learning techniques for inverse problems in imaging,"
   IEEE J. Sel. Areas Inf. Theory 1, 39–56 (2020).
- 144C. Bressler and M. Chergui, "Ultrafast x-ray absorption spectroscopy," Chem. Rev. 104, 1781–1812 (2004).
- 145H. Saisho and Y. Gohshi, Applications of Synchrotron Radiation to Materials Analysis (Elsevier, 1996).
- 146J. J. Rehr and R. C. Albers, "Theoretical approaches to x-ray absorption fine structure," Rev. Mod. Phys. 72, 621 (2000).
- 147 J. J. Rehr et al., "Ab initio theory and calculations of x-ray spectra," C. R. Phys. 10, 548–559 (2009).

- <sup>148</sup>J. J. Rehr, J. J. Kas, F. D. Vila, M. P. Prange, and K. Jorissen, "Parameter-free calculations of X-ray spectra with FEFF9," Phys. Chem. Chem. Phys. 12, 5503–5513 (2010).
- 149J. Terry et al., "Analysis of extended X-ray absorption fine structure (EXAFS) data using artificial intelligence techniques," Appl. Surf. Sci. 547, 149059 (2021).
- 150°C. Zheng et al., "Automated generation and ensemble-learned matching of x-ray absorption spectra," npj Comput. Mater. 4, 12 (2018).
- 151M. R. Carbone, S. Yoo, M. Topsakal, and D. Lu, "Classification of local chemical environments from x-ray absorption spectra using supervised machine learning," Phys. Rev. Mater. 3, 033604 (2019).
- 152S. B. Torrisi et al., "Random forest machine learning models for interpretable x-ray absorption near-edge structure spectrum-property relationships," npj Comput. Mater. 6, 109 (2020).
- 153M. R. Carbone, M. Topsakal, D. Lu, and S. Yoo, "Machine-learning x-ray absorption spectra to quantitative accuracy," Phys. Rev. Lett. 124, 156401 (2020).
- 154J. Gilmer, S. S. Schoenholz, P. F. Riley, O. Vinyals, and G. E. Dahl, "Neural message passing for quantum chemistry," Proc. Int. Conf. Mach. Learn. 70, 1263–1272 (2017).
- 155M. M. M. Madkhali, C. D. Rankine, and T. J. Penfold, "The role of structural representation in the performance of a deep neural network for x-ray spectroscopy," Molecules 25, 2715 (2020).
- 156°C. D. Rankine, M. M. M. Madkhali, and T. J. Penfold, "A deep neural network for the rapid prediction of x-ray absorption spectra," J. Phys. Chem. A 124, 4263–4270 (2020).
- 157 J. Timoshenko, D. Lu, Y. Lin, and A. I. Frenkel, "Supervised machine-learning-based determination of three-dimensional structure of metallic nanoparticles," J. Phys. Chem. Lett. 8, 5091–5098 (2017).
- 158J. Timoshenko and A. I. Frenkel, "Inverting x-ray absorption spectra of catalysts by machine learning in search for activity descriptors," ACS Catal. 9, 10192–10211 (2019).
- 159 A. A. Guda et al., "Quantitative structural determination of active sites from in situ and operando XANES spectra: From standard ab initio simulations to chemometric and machine learning approaches," Catal. Today 336, 3–21 (2019)
- 160 Y. Liu et al., "Mapping XANES spectra on structural descriptors of copper oxide clusters using supervised machine learning," J. Chem. Phys. 151, 164201 (2019).
- <sup>161</sup>N. Marcella et al., "Neural network assisted analysis of bimetallic nanocatalysts using X-ray absorption near edge structure spectroscopy," Phys. Chem. Chem. Phys. 22, 18902–18910 (2020).
- 162O. Trejo et al., "Elucidating the evolving atomic structure in atomic layer deposition reactions with in situ XANES and machine learning," Chem. Mater. 31, 8937–8947 (2019).
- 163S. Suga and A. Sekiyama, Photoelectron Spectroscopy: Bulk and Surface Electronic Structures (Springer, 2013).
- 164S. Hofmann, Auger- and X-Ray Photoelectron Spectroscopy in Materials Science: A User-Oriented Guide (Springer, 2013).
- 165 A. Aarva, V. L. Deringer, S. Sainio, T. Laurila, and M. A. Caro, "Understanding x-ray spectroscopy of carbonaceous materials by combining experiments, density functional theory, and machine learning. Part II: Quantitative fitting of spectra," Chem. Mater. 31, 9256–9267 (2019).
- 166G. Drera, C. M. Kropf, and L. Sangaletti, "Deep neural network for x-ray photoelectron spectroscopy data analysis," Mach. Learn. Sci. Technol. 1, 015008 (2020).
- 167K. Medjanik et al., "Direct 3D mapping of the Fermi surface and Fermi velocity," Nat. Mater. 16, 615 (2017).
- 168 S. Moser, "An experimentalist's guide to the matrix element in angle resolved photoemission," J. Electron Spectrosc. 214, 29–52 (2017).
   169 Y. He, Y. Wang, and Z. X. Shen, "Visualizing dispersive features in 2D image
- Y. He, Y. Wang, and Z. X. Shen, "Visualizing dispersive features in 2D image via minimum gradient method," Rev. Sci. Instrum. **88**, 073903 (2017).
- <sup>170</sup>H. Peng et al., "Super resolution convolutional neural network for feature extraction in spectroscopic data," Rev. Sci. Instrum. 91, 033905 (2020).
- <sup>177</sup>R. P. Xian et al., "A machine learning route between band mapping and band structure," arXiv:2005.10210 (2020).

- 172A. Furrer, T. Strassle, and J. Mesot, Neutron Scattering in Condensed Matter Physics (World Scientific, 2009).
- 1773 F. Fernandez-Alonso and D. L. Price, Neutron Scattering Magnetic and Quantum Phenomena (Academic Press, 2015).
- 174G. L. Squires, Introduction to the Theory of Thermal Neutron Scattering (Cambridge University Press, 1978).
- 175G. Shirane, S. M. Shapiro, and J. M. Tranquada, Neutron Scattering with a Triple-Axis Spectrometer: Basic Techniques (Cambridge University Press, 2002)
- <sup>176</sup>B. Dorner, Coherent Inelastic Neutron Scattering in Lattice Dynamics (Springer-Verlag, 1982).
- 177H. Sinn, "Spectroscopy with meV energy resolution," J. Phys. Condens. Mat. 13, 7525–7537 (2001).
- 178 E. Burkel, "Determination of phonon dispersion curves by means of inelastic x-ray scattering," J. Phys. Condens. Mat. 13, 7627–7644 (2001).
- 179 T. Nguyen et al., "Topological singularity induced chiral Kohn anomaly in a Weyl semimetal," Phys. Rev. Lett. 124, 236401 (2020).
- 180 M. Born and K. Huang, Dynamical Theory of Crystal Lattices (Clarendon Press, 1988).
- 181S. N. Taraskin and S. R. Elliott, "Phonons in vitreous silica: Dispersion and localization," Europhys. Lett. 39, 37–42 (1997).
- 182V. N. Novikov and N. V. Surovtsev, "Spatial structure of boson peak vibrations in glasses," Phys. Rev. B 59, 38–41 (1999).
- 183A. I. Chumakov et al., "Collective nature of the boson peak and universal transboson dynamics of glasses," Phys. Rev. Lett. 92, 245508 (2004).
- <sup>184</sup>H. Shintani and H. Tanaka, "Universal link between the boson peak and transverse phonons in glass," Nat. Mater. 7, 870–877 (2008).
- 185 A. I. Chumakov et al., "Equivalence of the boson peak in glasses to the transverse acoustic van Hove singularity in crystals," Phys. Rev. Lett. 106, 225501 (2011)
- 186j. B. Sokoloff, "Theory of inelastic neutron scattering in the itinerant model antiferromagnetic metals. I," Phys. Rev. 185, 770–782 (1969).
- 187S. H. Lee et al., "Emergent excitations in a geometrically frustrated magnet," Nature 418, 856–858 (2002).
- 188J. S. Helton et al., "Spin dynamics of the spin-1/2 kagome lattice antiferromagnet ZnCu3(OH)6Cl2," Phys. Rev. Lett. 98, 107204 (2007).
- 189 A. Banerjee et al., "Neutron scattering in the proximate quantum spin liquid α-RuCl<sub>3</sub>," Science 356, 1055–1058 (2017).
- <sup>190</sup>M. Eschrig, "The effect of collective spin-1 excitations on electronic spectra in high-T-c superconductors," Adv. Phys. 55, 47–183 (2006).
- <sup>191</sup>A. D. Christianson *et al.*, "Unconventional superconductivity in Ba(0.6)K(0.4)Fe2As2 from inelastic neutron scattering," Nature **456**, 930–932 (2008).
- 192 Y. Li et al., "Hidden magnetic excitation in the pseudogap phase of a high-T(c) superconductor," Nature 468, 283–285 (2010).
- 193 Z. Chen et al., "Direct prediction of phonon density of states with Euclidean neural networks," Adv. Sci. 2021, 2004214.
- 194G. Petretto et al., "High-throughput density-functional perturbation theory phonons for inorganic materials," Sci. Data 5, 180065 (2018).
- phonons for inorganic materials," Sci. Data 5, 180065 (2018).
   <sup>195</sup>T. E. Smidt, M. Geiger, and B. K. Miller, "Finding symmetry breaking order parameters with Euclidean neural networks," arXiv:2007.02005 (2020). Phys. Rev. Research 3, L012002 (2021).
- 196S. Toth and B. Lake, "Linear spin wave theory for single-Q incommensurate magnetic structures," J. Phys. Condens. Matter 27, 166002 (2015).
- 197Y. Li, W. Cheng, L. H. Yu, and R. Rainer, "Genetic algorithm enhanced by machine learning in dynamic aperture optimization," Phys. Rev. Accel. Beams 21, 054601 (2018).
- 198S. C. Leemann et al., "Demonstration of machine learning-based model-independent stabilization of source properties in synchrotron light sources," Phys. Rev. Lett. 123, 194801 (2019).
- 199J. Wan, P. Chu, Y. Jiao, and Y. Li, "Improvement of machine learning enhanced genetic algorithm for nonlinear beam dynamics optimization," Nucl. Instrum. Methods Phys. Res. Sect. A 946, 162683 (2019).
- 200 M. Piekarski, J. Jaworek-Korjakowska, A. I. Wawrzyniak, and M. Gorgon, "Convolutional neural network architecture for beam instabilities identification in synchrotron radiation systems as an anomaly detection problem," <u>Measurement</u> 165, 108116 (2020).

- 201 A. Sanchez-Gonzalez et al., "Accurate prediction of X-ray pulse properties from a free-electron laser using machine learning," Nat. Commun. 8, 15461 (2017).
- 202A. Asahara et al., "Early-stopping of scattering pattern observation with Bayesian modeling," Proc. AAAI Conf. Artif. Intell. 33, 9410–9415 (2019).
- <sup>203</sup>T. Kanazawa, A. Asahara, and H. Morita, "Accelerating small-angle scattering experiments with simulation-based machine learning," J. Phys. Mater. 3, 015001 (2019).
- 204 M. M. Noack et al., "A kriging-based approach to autonomous experimentation with applications to x-ray scattering," Sci. Rep. 9, 11809 (2019).
- 205 M. M. Noack, G. S. Doerk, R. Li, M. Fukuto, and K. G. Yager, "Advances in kriging-based autonomous x-ray scattering experiments," Sci. Rep. 10, 1325 (2020).
- <sup>206</sup>N. Cressie, "The origins of kriging," Math. Geol. **22**, 239–252 (1990).
- 207C. E. Rasmussen and C. K. I. Williams, Gaussian Processes for Machine Learning (MIT Press, 2006).
- 208X. Yang, F. De Carlo, C. Phatak, and D. Gürsoy, "A convolutional neural network approach to calibrating the rotation axis for x-ray computed tomography," J. Synchrotron Radiat. 24, 469–475 (2017).
- 209S. Lee et al., "Deep learning for high-resolution and high-sensitivity interferometric phase contrast imaging," Sci. Rep. 10, 9891 (2020).
- 210 C. Shashank Kaira et al., "Automated correlative segmentation of large transmission x-ray microscopy (TXM) tomograms using deep learning," Mater. Charact. 142, 203–210 (2018).
- 2<sup>11</sup>Y. Hui and Y. Liu, "Volumetric data exploration with machine learning-aided visualization in neutron science," Adv. Comput. Vision 943, 257–271 (2020).
- 212X. Yang et al., "Low-dose x-ray tomography through a deep convolutional neural network," Sci. Rep. 8, 2575 (2018).
- <sup>213</sup>R. Zhang, Y. Liu, and H. Sun, "Physics-informed multi-LSTM networks for metamodeling of nonlinear structures," Comput. Methods Appl. Mech. Eng. 369, 113226 (2020).
- <sup>214</sup>E. Flurin, L. S. Martin, S. Hacohen-Gourgy, and I. Siddiqi, "Using a recurrent neural network to reconstruct quantum dynamics of a superconducting qubit from physical observations," Phys. Rev. X 10, 011006 (2020).
- 215 C. Roth, "Iterative retraining of quantum spin models using recurrent neural networks," arXiv:2003.06228 (2020).
- 216 A. Deng, J. Huang, H. Liu, and W. Cai, "Deep learning algorithms for temperature field reconstruction of nonlinear tomographic absorption spectroscopy," Meas. Sens. 10–12, 100024 (2020).
- 217 L. Simine, T. C. Allen, and P. J. Rossky, "Predicting optical spectra for optoelectronic polymers using coarse-grained models and recurrent neural networks," Proc. Natl. Acad. Sci. U.S.A. 117, 13945–13948 (2020).
- 218°C. Tian *et al.*, "Deep learning on image denoising: An overview," Neural Netw. 131, 251–275 (2020).
- <sup>219</sup>M. Deng, S. Li, A. Goy, I. Kang, and G. Barbastathis, "Learning to synthesize: Robust phase retrieval at low photon counts," Light Sci. Appl. 9, 36 (2020).
- 220 A. Goy, K. Arthur, S. Li, and G. Barbastathis, "Low photon count phase retrieval using deep learning," Phys. Rev. Lett. 121, 243902 (2018).
- 221 Z. Che, S. Purushotham, K. Cho, D. Sontag, and Y. Liu, "Recurrent neural networks for multivariate time series with missing values," Sci. Rep. 8, 6085 (2018)
- 222 R. T. Chen, Y. Rubanova, J. Bettencourt, and D. Duvenaud, "Neural ordinary differential equations," arXiv:1806.07366 (2018).
- 223K. Hashimoto, H.-Y. Hu, and Y.-Z. You, "Neural ODE and holographic QCD," arXiv:2006.00712 (2020).
- 224M. Nakajima, K. Tanaka, and T. Hashimoto, "Neural Schrödinger equation: Physical law as neural network," arXiv:2006.13541 (2020).
- 225B. Lusch, J. N. Kutz, and S. L. Brunton, "Deep learning for universal linear embeddings of nonlinear dynamics," Nat. Commun. 9, 4950 (2018).
- <sup>226</sup>K. Champion, B. Lusch, J. N. Kutz, and S. L. Brunton, "Data-driven discovery of coordinates and governing equations," Proc. Natl. Acad. Sci. U.S.A. 116, 22445–22451 (2019).
- 227J. Ngiam et al., "Multimodal deep learning," in Proceedings of the 28th International Conference on Machine Learning (Association for Computing Machinery, 2011), pp. 689–696.
- <sup>228</sup>K. Sohn, W. Shang, and H. Lee, "Improved multimodal deep learning with variation of information," Adv. Neur. Inform. Proc. Syst. 27, 2141–2149 (2014).

- 229T. Baltrušaitis, C. Ahuja, and L.-P. Morency, "Multimodal machine learning: A survey and taxonomy," IEEE Trans. Pattern Anal. Mach. Intell. 41, 423–443 (2019).
- <sup>230</sup>K. Liu, Y. Li, N. Xu, and P. Natarajan, "Learn to combine modalities in multi-modal deep learning," arXiv:1805.11730 (2018).
- 231 V. Radu et al., in Proceedings of the 2016 ACM International Joint Conference on Pervasive and Ubiquitous Computing: Adjunct (Association for Computing Machinery, 2016), pp. 185–188.
- <sup>232</sup>V. Radu *et al.*, "Multimodal deep learning for activity and context recognition," Proc. ACM Interact. Mob. Wearable Ubiquitous Technol. 1, 157 (2018).
- <sup>233</sup>A. Eitel, J. T. Springenberg, L. Spinello, M. Riedmiller, and W. Burgard, in 2015 IEEE/RSJ International Conference on Intelligent Robots and Systems (IROS) (IEEE, 2015), pp. 681–687.
- <sup>234</sup>D. Hong et al., "More diverse means better: Multimodal deep learning meets remote-sensing imagery classification," IEEE Trans. Geosci. Remote Sens. 59, 4340–4354 (2020).
- 235W. Liu, W.-L. Zheng, and B.-L. Lu, in International Conference on Neural Information Processing (Springer, 2015), pp. 521–529.
- <sup>236</sup>M. Liang, Z. Li, T. Chen, and J. Zeng, "Integrative data analysis of multiplatform cancer data with a multimodal deep learning approach," IEEE/ACM Trans. Comput. Biol. Bioinform. 12, 928–937 (2015).
- 237T. Xu, H. Zhang, X. Huang, S. Zhang, and D. N. Metaxas, in *International Conference on Medical Image Computing and Computer-Assisted Intervention* (Springer, 2016), pp. 115–123.
- 238G. Carleo and M. Troyer, "Solving the quantum many-body problem with artificial neural networks," Science 355, 602–606 (2017).
- <sup>239</sup>O. A. Von Lilienfeld, K.-R. Müller, and A. Tkatchenko, "Exploring chemical compound space with quantum-based machine learning," Nat. Rev. Chem. 4, 347–358 (2020).
- <sup>240</sup>M. S. Hybertsen and S. G. Louie, "First-principles theory of quasiparticles: Calculation of band gaps in semiconductors and insulators," Phys. Rev. Lett. 55, 1418–1421 (1985).

- <sup>241</sup>V. I. Anisimov, A. I. Poteryaev, M. A. Korotin, A. O. Anokhin, and G. Kotliar, "First-principles calculations of the electronic structure and spectra of strongly correlated systems: Dynamical mean-field theory," J. Phys. Condens. Matter 9, 7359–7367 (1997).
- <sup>242</sup>A. Georges and G. Kotliar, "Hubbard model in infinite dimensions," Phys. Rev. B 45, 6479–6483 (1992).
- 243K. Haule and G. Kotliar, "Coherence-incoherence crossover in the normal state of iron oxypnictides and importance of Hund's rule coupling," New J. Phys. 11, 025021 (2009).
- 2444H. Park, K. Haule, and G. Kotliar, "Magnetic excitation spectra in BaFe2As2: A two-particle approach within a combination of the density functional theory and the dynamical mean-field theory method," Phys. Rev. Lett. 107, 137007 (2011).
- 245 A. Hariki, M. Winder, T. Uozumi, and J. Kuneš, "LDA+DMFT approach to resonant inelastic x-ray scattering in correlated materials," Phys. Rev. B 101, 115130 (2020).
- <sup>246</sup>Q. Li, J. Callaway, and L. Tan, "Spectral function in the two-dimensional Hubbard model," Phys. Rev. B 44, 10256–10269 (1991).
- 247R. J. Bartlett and M. Musiał, "Coupled-cluster theory in quantum chemistry," Rev. Mod. Phys. 79, 291–352 (2007).
- <sup>248</sup>S. R. White and A. E. Feiguin, "Real-time evolution using the density matrix renormalization group," Phys. Rev. Lett. 93, 076401 (2004).
- <sup>249</sup>W. M. C. Foulkes, L. Mitas, R. J. Needs, and G. Rajagopal, "Quantum Monte Carlo simulations of solids," Rev. Mod. Phys. 73, 33–83 (2001).
- 250 S. M. Winter et al., "Breakdown of magnons in a strongly spin-orbital coupled magnet," Nat. Commun. 8, 1152 (2017).
- 251 E. W. Huang et al., "Numerical evidence of fluctuating stripes in the normal state of high-T<sub>c</sub> cuprate superconductors," Science 358, 1161–1164 (2017).